A reverse-central-dogma pathway underlies ribosome-antibiotic efficacy and accelerates resistance evolution

Yayun Zheng[1]#, Ruochen Chai[1]#, Zeqi Xu[1], Yihui He[1], Ping Shen[1], Jintao Liu[1,2]*, Tianmin Wang[3]*

[1] Center for Infectious Disease Research, School of Medicine, Tsinghua University, Beijing 100084, China

[2] Tsinghua-Peking Center for Life Sciences, Beijing 100084, China

[3] School of Life Science and Technology, ShanghaiTech University, Shanghai 201210, China

#These authors contributed equally to this work

*Address correspondence to Jintao Liu, jintaoliu@tsinghua.edu.cn

*Address correspondence to Tianmin Wang, wangtm@shanghaitech.edu.cn

Abstract

In bacteria, the precise coordination of DNA replication, transcription and translation is mediated by dynamic interactions among the corresponding macromolecular machineries, playing a pivotal role in maintaining cellular homeostasis. Here we show that such coordination is hijacked by ribosome antibiotics to trigger secondary damage that predominantly contributes to their efficacy. Specifically, through developing a transcription dynamics profiling method, complemented by genetic and biochemical approaches, we unveil that translation inhibition disrupts transcription-translation coupling, leading to premature stalling of RNA polymerase (RNAP) at genome scale, which subsequently triggers extensive genomic instability. Moreover, mutagenic repairment of genomic lesions is mediated by heterogenous hyperactivation of SOS response, facilitating an inducible evolutionary path towards genetic resistance characterized by a unique mutation spectrum. Our findings thereby reveal a yet overlooked reverse-central-dogma pathway underlying actions of ribosome inhibitors, and establish a framework to understand antibiotic efficacy and induced mutagenesis through network disorder.

Introduction

Antibiotic treatment is the most effective strategy to combat bacterial infections. Unfortunately, many antibiotics are nullified by the rapid emergence of bacteria that exhibit tolerance or even resistance[1–5]. Compounding this issue is the dwindling rate of new antibiotic discovery[6]. In this context, to improve eradication and minimize the likelihood of resistance evolution, it is crucial to unravel the molecular mechanisms underlying the emergent tolerance and resistance, so as to optimize protocols for the administration of existing drugs.

While significant progress has been made in elucidating the primary macromolecular targets of antibiotics, these atomic interactions alone do not fully elucidate the intricate mechanisms underlying bacterial killing or resistance evolution. Beyond the primary target binding, what is largely unknown and exceedingly complex, are the subsequent molecular procedures that mediate secondary damages and activate stress responses[7–11], which ultimately determine the outcome of drug treatment[12]. The reason for this is that biological networks are interwoven, and antibiotic perturbation may disrupt their intricate coordination[13], resulting in enhanced secondary destruction affecting vital pathways beyond the primary target. Hence, the coordination of biological networks crucial for cellular homeostasis could be potentially leveraged by antibiotics as an efficacy amplifier.

In bacteria, tight coordination of DNA replication, transcription and translation is mediated by dynamic physical interactions among macromolecular machineries[14–16]. Functionally, such coordination is crucial for maintaining cellular homeostasis[17–19]. For example, trailed ribosomes

chase the elongating RNA polymerase (RNAP)[14,20], and such transcription-translation coupling (TTC) contribute to RNAP processivity[21–23]. While RNAPs are reported to maintain genomic stability as lesion scanners[24], when conflicting with DNA replication machineries, they in turn cause DNA damage[25,26]. Therefore, disruption of any link in this chain may lead to the breakdown of cellular homeostasis and the ultimate killing of bacteria in the context of antibiotics treatment. Moreover, once the secondary effects compromise genome integrity, survivors have a high propensity for rapid genotypic resistance evolution through error-prone DNA repair[27,28].

Ribosome inhibitors, targeting on translation machinery, constitute over half of drugs in clinical treatment of bacterial infections[29]. Despite their medical importance, the molecular procedures underlying the efficacy of these drugs, especially how initial ribosome binding induces secondary damage culminating in bacterial killing, largely remain elusive[12,30–32]. To address this gap, we propose that a systems biology approach encompassing the disordered macromolecule interplay, as described above, represents a fundamental yet overlooked direction. Here, utilizing genetic and biochemical techniques, coupled with a novel deep-sequencing-based transcription dynamics profiling method, we unveil a universal reverse-central-dogma pathway that links initial ribosome inhibition to ultimate DNA damage, which is mediated by the disruption of TTC and subsequent premature RNAP stalling at genome scale. This pathway leads to strong variability at single cell level, ranging from phenotypic tolerance to cellular death. Among the survived minority, resistance evolution is propelled by induced mutagenesis. Our results show how clinically relevant pharmaceutical interventions perturb the precise coordination between macromolecular machineries, leading to unforeseen cellular consequences that underlie drug efficacy and expedite

genetic diversification. Broadly, our works set out a path to understand drug tolerance and resistance evolution from a network biology perspective.

Results

A rapid switch from phenotypic tolerance to genetic resistance under gentamicin treatment

We first focused on gentamicin, an aminoglycoside antibiotic that belongs to a large family of ribosome-targeting antibiotics known for their bactericidal effects and extensive use in current medicine[33]. Specifically, we employed a model system in which we treated exponential-phase *E. coli* cultures with 6 mg/L gentamicin to investigate potential secondary effects of the drug beyond its primary ribosome binding. Note that this concentration is around two-fold the minimal inhibitory concentration (MIC) in our experimental setting and clinically relevant[34,35]. Bacterial growth was arrested by gentamicin treatment within one hour, according to the OD_{600} readout, followed by a gradual decline in biomass, indicating cellular death and lysis (**Figure 1a**). Indeed, the killing assay (**Methods**) suggested that the bacteria started to be killed around 40 minutes after drug treatment, with the number of surviving bacteria gradually decreasing until approximately 90 minutes, at which point 99.9% of cells were killed (**Figure 1b**).

Interestingly, the killing process abruptly halted around 90 minutes, and a small population persisted (**Figure 1b**). This phenomenon is commonly implicated as phenotypic persistence, which is genetically not heritable[1]. To investigate the survival modes during drug treatment and especially whether they were genetically heritable, we employed a highly sensitive drug susceptibility assay[36] (**Methods**, **Figure 1c**). In particular, we systematically profiled 48 isolates

recovered from 12 time points during gentamicin treatment: their growths under a series of gentamicin concentrations were quantified by calculating the area under curve (AUC) of OD_{600} readout (**Figure 1c**). Surprisingly, we identified the emergence of genetically heritable tolerance and even resistance soon after drug treatment (**Figure 1d**) (see **Methods** for the definitions of different survival modes).

In particular, clones with prolonged lag time, indicating genotypic tolerance[37], emerged as early as one hour after drug treatment (**Figure 1d**, No. 11 isolate from t_3 sample, **Supplementary Figure 1a**), and continuously accumulated from 1.3 hours to 3.4 hours of drug treatment (**Figure 1d**, isolates from samples $t_4 \sim t_9$). More remarkably, strains exhibiting genotypic resistance appeared as early as 1.3 hours after drug treatment (**Figure 1d**, No. 15 isolate from t_4 sample). Moreover, the proportion of isolates with genotypic resistance gradually increased among the surviving bacteria, became dominant at 2.2 hours (**Figure 1d**, 3/5 in t_7 sample) and completely took over the population by 5.3 hours (**Figure 1d**, 4/4 in t_{10} sample) after drug treatment. Consistent with the genetic resistance hypothesis, we frequently (> 90%) observed a recovery of growth after 12-hour treatment by 6 mg/L gentamicin (**Figure 1a**), indicating the evolution and growth of the resistant mutants in the presence of drugs.

To validate the emergence of genetic alternations that gave rise to tolerance or resistance, we adopted genome re-sequencing to identify mutations present in the isolates. In agreement with our hypothesis, we identified at least one mutation in each of the eight selected isolates (one mutation in 7/8, two in 1/8 isolates) (**Figure 1d**). Functionally, these mutations ranged from stress response

to respiration, and many of the corresponding genes have been previously implicated in gentamicin resistance[38,39]. These results showed that tolerant and resistant mutants with very high genetic diversity could emerge within a very short period of time, engaging in competitions where the advantageous ones ultimately thrive. Taken together, our results demonstrate a swift transition in survival modes, progressing from phenotypic tolerance (< 90 min) to intermediately genotypic tolerance (1.0 h ~ 3.4 h), and finally genotypic resistance dominates within a few hours under clinically relevant[34,35] gentamicin eradication.

Gentamicin triggers genomic instability and inducible evolution

The rapid emergence of mutants under gentamicin treatment suggests a potential mechanism of induced mutagenesis. Actually, in most of the cases (21/25), the resistant mutants exhibited severe growth defects in the absence of gentamicin (**Figure 1d**, **Supplementary Figure 1b**, **1d**), indicating that they were less likely to exist prior to treatment due to strong negative selection. To investigate the possibility of induced mutagenesis, we turned to SOS responses, a genetic program commonly encoded in bacterial genomes, which is triggered by DNA damage and potentially performs error-prone DNA lesion repair[40]. Agreeing with our assumption, transcriptomic analysis revealed activation of SOS responses (**Figure 2a**), occurring between 40 minutes and 60 minutes, coinciding with the onset of bacterial death (**Figure 1b**). Furthermore, we directly measured DNA damage that triggers SOS responses. Specifically, we employed TUNEL assays to detected DNA lesions[31] (**Supplementary Figure 2a-2c**); The ratio of TUNEL-positive cells substantially increased after 40 minutes of gentamicin treatment and peaked at 60 minutes (**Figure 2b**). Therefore, we concluded that gentamicin treatment dramatically damaged DNA and triggered global SOS responses.

Since SOS responses repair DNA in a mutagenic manner, we should be able to find the characteristic mutations. We isolated mutants following three hours or longer gentamicin treatment (**Methods**); Genome re-sequencing identified at least one mutation in each isolate, amounting to a total of 35 non-duplicated mutations (**Supplementary Table 1**, **Figure 2c**). As a reference, we regarded the 21 genetic variation loci in our wildtype strain compared with the reference genome of *E. coli* K12 (NC000913.3) as spontaneous mutations (**Supplementary Table 2**, **Figure 2d**). These mutations were assumed to have been accumulated during endogenous DNA replication. Interestingly, we observed distinct patterns between these two mutation spectra (**Figure 2e**, **2f**).

Particularly, mutations resulting from gentamicin treatment exhibited an increase in structural variants like insertion sequence (IS) and deletions (**Figure 2e**). These signatures are associated with recombination during DNA damage repair[41]. Consistently, the expressions of transposase genes of relevant ISs arose since 60~90 minutes after gentamicin treatment (**Supplementary Figure 3a**), just before the emergence of genotypic tolerance or resistance. Additionally, the appearance of Δ1 bp deletion is known to be frequently generated during translesion synthesis by DNA Pol IV (DinB)[42], which is activated during SOS responses upon gentamicin treatment (**Figure 2a**, **Supplementary Figure 3b**).

Besides structural variants, the patterns of base pair substitutions (BPS) also exhibited notable differences between these two groups of mutations (**Figure 2e**, **2f**). In spontaneous mutations, transitions (60%) were more prevalent compared with transversions (40%). By contrast, we

identified more transversions (58.8%) compared with transitions (41.2%), which aligns with a recently reported characteristic of SOS-induced mutagenesis[43]. Among the transversions observed in the gentamicin-treated group, akin to Δ1 bp deletions mentioned earlier, the emergence of A:T→C:G substitutions is known to be derived from DinB-dependent translesion synthesis[42]. Additionally, G:C→T:A transversions are known to be caused by genotoxic 8-oxo-deoxyguanine (8-oxo-dG) species formed during oxidative stresses; Foti et al. previously reported that gentamicin treatment induces cellular oxidative stresses and damaged DNA[31]. In our case, however, 8-oxo-dG only showed minor contribution to the mutations recovered from gentamicin treatment (4/10 among transversions, **Figure 2e**).

Together, these results suggest an inducible mutagenesis pathway that is triggered by gentamicin and appears to be largely independent of 8-oxo-dG. In line with this, deleting genes encoding these error-prone translesion DNA polymerases (*polB*, *dinB* and *umuC*) impaired bacterial tolerance three hours after drug treatment (**Supplementary Figure 3c**), where survivors were dominated by genetic resistance (**Figure 1d**).

Gentamicin treatment gives rise to genome-wide premature RNAP stalling

We next sought to reveal how proteotoxic gentamicin triggers genomic instability and mutagenesis. An intriguing observation in the transcriptomics data provided an initial clue – gentamicin treatment resulted in a pronounced decrease in RNA-seq coverage towards the 3' ends of many genes, particularly those loci where inducible mutations were frequently detected (**Figure 2g**, **2h**). This finding suggested a potential compromise in RNA polymerase (RNAP) elongation

processivity and pervasive occurrence of **p**remature **R**NAP **s**talling **e**vents (PRSEs). As PRSEs and associated molecular events are detrimental to genomic stability[44,45], a cellular consequence of gentamicin treatment as shown above, we determined to investigate PRSEs on systems level. To this end, we adopted a transcription dynamics profiling method, referred to as 3'-end-seq, which allowed us to globally dissect 3' ends of bacterial transcripts with single-nucleotide resolution (**Figure 3a**, **Methods**). As expected, our 3'-end-seq reliably identified known intrinsic termination events, confirming normal RNAP elongation in the absence of gentamicin perturbation (**Figure 2g**, **2h**, upper panel; see **Supplementary Figure 4** for the validation of 3'-end-seq accuracy). Using this method, we defined PRSEs as emergent RNA 3' ends exclusively occurring within the gene-coding regions (**Methods**, **Supplementary Figure 5**). The underlying assumption is that these emergent RNA termini predominantly originate from PRSEs, thus their profiles can serve as a reflection of dysfunctional RNAP elongation at genome scale.

In the presence of antibiotics, for both *cpxRA* and *hemL* operon, where normal RNA-seq exhibited coverage bias towards the 5' ends of the operon (**Figure 2g**, **2h**), 3'-end-seq indeed identified substantial PRSEs occurring abnormally within the gene-coding regions (**Figure 3b**, **3c**). Here, we observed either one dominant PRSE (*cpxRA*, **Figure 3b**) or multiple minor PRSEs with comparable intensities (*hemL*, **Figure 3c**). To quantitatively dissect global PRSEs during drug treatment, we developed two computational statistics. The first statistic counted the number of predominant PRSEs surpassing a predefined "enrichment" threshold (**Methods**), while the second statistic, referred to as PRSE intensity, quantified the total intensity of PRSEs in each gene (**Methods**). Using these two statistics, we showed that both the number of predominant PRSEs (**Figure 3d**) and the gene-wise PRSE intensity (**Figure 3e**) increased after gentamicin treatment.

Quantitatively, the total number of predominant PRSEs increased threefold after 110 minutes of treatment compared to the initial time point (**Figure 3d**); Moreover, the PRSE intensity increased by more than 1.5-fold among 41.9 % of all genes after 60 minutes of gentamicin treatment (**Figure 3e**). In terms of timing, PRSEs substantially boosted after 40 min drug treatment (**Figure 3d**, **Supplementary Figure 6**), which coincided with or slightly preceded the occurrence of genomic instability (**Figure 2b**) and cellular death (**Figure 1b**), indicating a potential link with these downstream molecular events.

To further substantiate our assertion that 3'-end-seq effectively detected PRSEs, we aimed to genetically manipulate RNAP elongation dynamics. To this end, we deleted *mfd*, which encodes a DNA translocase that recognizes and rescues stalled RNAP, by promoting its forward translocation[46]. Indeed, *mfd* knockout globally promoted PRSEs even in the absence of gentamicin treatment (0 min from **Figure 3f**, **Figure 3g**). Notably, in many loci, *mfd* deletion led to a significantly higher occurrence of PRSEs compared to the wildtype strain following exposure to gentamicin (60 min from **Figure 3f**, **Supplementary Figure 7**). PRSEs can also be indirectly quantified by the amount of R-loop[47], a DNA:RNA hybrid structure generated from nascent transcripts persisting in template DNA, which is associated with stalled RNAPs[45,48]. We observed strengthened R-loop formation 30 min after gentamicin treatment (**Figure 3i**), consistent with increase in PRSE intensities characterized by 3'-end-seq (**Figure 3d**). Furthermore, *mfd* knockout leads to augmented R-loop formation than wildtype without or upon gentamicin treatment (**Figure 3i**). Overall, these findings confirm 3'-end-seq as a reliable assay to profile transcription dynamics and to identify PRSEs. Through this method, we depict that gentamicin treatment triggers genome-wide PRSEs.

Drug-induced PRSEs are responsible for DNA damage and mutagenesis

During gentamicin treatment, the co-occurrence of PRSEs (**Figure 3**) and genomic instability (**Figure 2**) implies a potential link between these two molecular phenomena. Indeed, RNAPs engage in intensive interactions with DNA replication and repair machinery; and the homeostasis of RNAP kinetics is crucial for preserving genome stability[18,49]. Moreover, DNA replication persists for 60 minutes after drug treatment (**Supplementary Figure 8**), allowing for possible conflicts between kinetically disordered RNAPs and other DNA-associated macromolecular complexes. Hence, we assumed that gentamicin-induced PRSEs are potent to trigger pervasive DNA damage (**Figure 2**).

To test this hypothesis, we genetically manipulated the occurrence of PRSEs and measured the resulting changes in DNA damage. Specifically, we boosted the abundance of PRSEs by deleting the transcription elongation factor Mfd[46,50,51], which is known to rescue PRSEs (**Figure 3f-i**). Indeed, slightly amplified lesions in genomic DNA under gentamicin was observed in Δ*mfd* strain using either the TUNEL assay (**Figure 4a**) or pulse-field gel electrophoresis (PFGE) assay (**Figure 4b**, **Supplementary Figure 9**, **Methods**). Conversely, genomic instability induced by gentamicin can be largely abolished by deleting the RNAP-binding helicase UvrD (**Figure 4c**), which has recently been implicated in promoting the backtracking of stalled RNAPs[24,52,53]. Similar mitigation of DNA damage were observed by knocking out *uvrB* or *uvrC* (**Figure 4c**), whose products are also associated with RNAP and carry out lesion scanning and DNA incision[49]. These results

suggest that, despite lacking specified mechanisms, RNAP-associated Uvr complex substantially contributes to DNA damage triggered by gentamicin.

Furthermore, we discovered that the cytotoxic effect of gentamicin is mediated by genotoxicity: altered levels of DNA damage resulting from the deletion of *mfd* or *uvrD*, respectively, led to decreased or increased survival rates in the killing assay compared to the wildtype strain (**Figure 4d**). Additionally, akin to *mfd* knockout, deleting any of any of the other PRSE-rescuing factors (*greA*, *greB*, *rnhA* and *rnhB*) caused a fitness defect under gentamicin treatment (**Figure 4f**), as measured by the drug susceptibility assay (**Methods**). Therefore, through the genetic manipulation of PRSE occurrence, we established a causal relation between PRSEs, DNA damage, and cellular death in the context of ribosome stress.

Given that DNA damages trigger the onset of mutagenic repair, and considering the established correlation between PRSEs and DNA damage, we postulate that regions harboring PRSEs may act as mutational hotspots within the genome. To test this hypothesis, we quantified PRSE intensities of coding genes harboring gentamicin-induced mutations (**Methods**, **Figure 2c**) or those genes where mutations occur spontaneously (**Figure 2d**). Consistent with our assumption, we observed substantially enhanced PRSEs surrounding mutations arising from gentamicin treatment compared to PRSEs associated with spontaneous mutations (**Figure 4f**). These findings further validate the proposed model, drug-induced PRSEs inflict damage to genomic DNA, which leads to induced mutagenesis, potentially through error-prone lesion repair.

PRSEs are caused by nascent RNA structures originally repressed by the coupled ribosome

After establishing a causal link between PRSEs and genomic instability, our next aim was to elucidate the mechanism underlying rapid PRSE emergence triggered by gentamicin, the final missing step about how this ribosome-binding drug unexpectedly gave rise to DNA damage and induced mutagenesis. In most bacteria, including *E. coli*, the rates of RNAP elongation and ribosome movement are precisely coordinated. This coordination ensures that RNAP is closely followed by a trailing ribosome[20], a process known as transcription-translation coupling (TTC). Functionally, TTC contributes to gene expression regulation and RNAP elongation[22,23]. Interestingly, working on a few operons, Zhu et al. showed that inhibiting translation compromised RNAP processivity potentially via disrupting TTC[22]; Furthermore, using a reconstituted in vitro system, Wee et al. recently showed that TTC accelerates RNAP elongation through force and allostery[23]. Building on these elegant studies, we investigated whether the genome-wide occurrence of PRSEs resulted from weakened RNAP processivity that was originally supported by coupled ribosomes.

In this line, we reasoned that following gentamicin treatment, large-scale PRSEs would only be observed on protein-coding genes, while noncoding genes, which lack translation, would not exhibit significant PRSEs. To test this hypothesis, we analyzed RNA-seq results using read coverage analysis (**Methods**). Prior to gentamicin treatment, both protein-coding and noncoding genes displayed a uniform read coverage distribution (**Figure 5a**, **5b**), indicating normal RNAP elongation. After 60 minutes of gentamicin treatment, read coverage on protein-coding genes showed a pronounced skewness towards the 5' ends (**Figure 5a**), suggesting dysfunctional RNAP elongation. Conversely, no such coverage polarity was observed on noncoding genes (**Figure 5b**).

To enhance the resolution of our analysis, we next turned to 3'-end-seq results. After rescaling the PRSE profile for each gene (**Methods**), we found that PRSEs were infrequent and randomly distributed on protein-coding genes in the absence of ribosome inhibition (**Figure 5c**), suggesting generally high RNAP processivity. However, gentamicin treatment dramatically disrupted this pattern, leading to the emergence of strong, positionally biased PRSEs (**Figure 5d**), indicative of significantly weakened RNAP processivity. In stark contrast to protein-coding genes, rare PRSEs were randomly distributed on noncoding genes, exhibiting no difference between drug treatment and no treatment (**Figure 5e**, **5f**). Hence, gentamicin leads to genome-wide PRSEs via directly inhibiting ribosome and disrupting TTC. Supporting this assertion, we also observed substantial PRSEs in many leader-peptide-regulated genes (**Supplementary Figure 10**), where TTC is known to play critical roles in gene expression regulation at transcriptional level[54].

The regional enrichment of PRSE pattern on protein-coding genes (**Figure 5d**) suggests that specific sequence contexts contribute to the emergence of PRSEs following TTC disruption. It has been postulated that the formation of nascent RNA hairpin structures promotes PRSEs, with this effect being largely inhibited by the closely coupled ribosome[55]. Hence, we investigated whether structured nascent RNAs formed during transcription play a role in the genome-wide occurrence of PRSEs after gentamicin treatment. Minimal folding energy (MFE) analysis of 50 nt upstream sequences of gentamicin-associated predominant PRSEs (**Methods**) revealed the formation of nascent RNA hairpins, as evidenced by more negative MFEs than random sequences (**Figure 5g**, 60 or 110 min vs. random). Intriguingly, we found that the MFEs of PRSE-associated nascent RNA hairpins following gentamicin treatment were significantly higher than those of intrinsic termination sites, which primarily mediate RNAP dissociation events under normal RNAP

processivity protected by the trailing ribosome (**Figure 5g**, 60 or 110 min vs. intrinsic termination). These results indicate that even less structured nascent RNAs are sufficient to induce PRSEs when protection from the coupled ribosome is absent.

Besides nascent RNA secondary structure, we also examined the contribution of transcription termination sequence signals to PRSEs (**Methods**). Consistently, while the canonical sequence signal (GC-rich hairpin plus polyU) was critical for intrinsic transcription termination events under normal RNAP processivity (**Figure 5h**), the dependence on this signal nearly disappeared after ribosome inhibition (**Figure 5i**, **5j**). These findings demonstrate that following drug treatment, RNAP processivity becomes more susceptible to even less-structured nascent RNAs lacking intrinsic transcription termination signals. Consequently, these pervasive structures, which would have been inhibited by the coupled ribosome, rapidly induce genome-wide PRSEs.

The reverse-central-dogma pathway determines ribosome antibiotics efficacy

To evaluate whether the pathway uncovered here (**Figure 6a**) extends beyond the specific characteristics of gentamicin and applies universally to translation inhibition, we investigated whether certain predicted effects from the proposed pathway could be observed with other ribosome-targeting antibiotics. First, we predicted that transcription elongation factors played critical roles in modulating bacterial fitness under proteotoxic stress induced by other ribosome antibiotics, such as gentamicin (**Figure 4a**). To test this, we assessed the fitness impact of *mfd* under treatment with a comprehensive panel of ribosome antibiotics, using the drug susceptibility assay (**Figure 1c**, **Methods**). Consistent with our assumption, *mfd* knockout gave rise to

substantial fitness defects when translation was inhibited, regardless of the specific drugs or their binding sites (**Figure 6b**). Next, we posited that DNA damage and SOS response would be observed when actively growing bacteria were challenged by different ribosome antibiotics, as demonstrated in the case of gentamicin (**Figure 2a-2b**). To test this prediction, we constructed a genetically encoded SOS reporter (**Methods**). Indeed, all tested ribosome-targeting drugs led to rapid activation of SOS responses (**Figure 6c**), indicating pervasive DNA damage in these cases.

Another prediction regarding this pathway concerns the presence of phenotypic heterogeneity at the single-cell level. Our rationale was that transcription at the single-molecule level exhibits stochastic behavior through bursting mechanisms[56], resulting in variable RNAP allocations across the genome. Consequently, this leads to divergent DNA damage profiles, repair activations, and cellular fates in individual cells. To examine the potential heterogeneity, we adopted the abovementioned SOS reporter (**Methods**) in combination with fluorescence activated cell sorting (FACS) to separate bacterial subpopulations with distinct SOS responses after 40 minutes of gentamicin treatment (**Figure 6d**). Interestingly, we found that the subpopulation with stronger SOS responses also exhibited three-fold enhancement in survival (**Figure 6e**), indicating the contribution of heterogenous PRSE-triggered DNA damage and repair activation to initial phenotypic tolerance (**Figure 1d**, **Methods**). This subpopulation, characterized by heightened DNA repair capacity and enhanced survival, may act as a reservoir for subsequent inducible evolution towards genetic resistance (**Figure 1d**, **Discussion**). Agreeing with our results in *E. coli*, hyperactivation of SOS responses in a subpopulation was also observed in clinical isolates of *Klebsiella pneumoniae* following gentamicin treatment, as revealed by a recently developed bacterial single-cell RNA sequencing (scRNA-seq) technology (**Supplementary Figure 11**).

Discussions

In this study, we elucidated a reverse-central-dogma pathway that governs the critical yet previously overlooked secondary effects of ribosome-targeting antibiotics (**Figure 6a**). This pathway originates from the acute disruption of widely spread TTC in bacteria, next dramatically inhibits the processivity of RNAP to trigger PRSE and R-loop formation at genome scale, thereby causing severe genomic instability. Consequently, the majority of bacteria succumb to cell death when the capacity for DNA repair is inadequate. Moreover, the induced error-prone DNA repair mechanisms accelerate the evolution of resistance, allowing the descendants of successful mutants to eventually dominate the population. Several insightful works have proposed that, in a conceptional model, perturbing translation can affect DNA stability via compromising RNAP processivity[25]. In the context of ribosome antibiotic treatment, our investigation substantiates this concept through a systematic examination at single-nucleotide resolution and genome scale, employing state-of-the-art technologies such as transcription dynamics profiling. This serves as an example of the domino effect, starting with primary ribosome inhibition and culminating in profound genomic damage, which establishes the key physiological effects of ribosome antibiotics. Moreover, our work underlay the importance to understand drug efficacy from a rarely explored perspective of disrupted coordination in biological networks[57]. Interestingly, Kaplan et al.[58] recently adopted a random network approach to elegantly model a perturbed cellular state following acute stress, conceptionally akin to the large-scale disorder in central dogma as described here. Better understanding about how cells enter, respond to, and exit these disordered states could shed new light on the survival and evolution of bacteria as well as tumors[59], during drug therapy.

It is imperative to note that we do not purport that the uncovered reverse-central-dogma pathway is the sole arbiter of ribosome antibiotic efficacy. As highlighted earlier, a systematic view is indispensable for comprehending drug efficacy. In the case of ribosome antibiotics, like aminoglycosides, other secondary effects, including ROS[9,30], also possess potential in mediating drug efficacy. Notably, the reverse-central-dogma pathway uncovered here exhibits relatively rapid kinetics compared to other functionally relevant processes like ROS. The global PRSEs manifest within 30 minutes and boost before one hour of gentamicin treatment (**Figure 3d**), with DNA damage exhibiting similar temporal patterns (**Figure 2b**). In contrast, ROS generation is slower. For instance, when applying 5 mg/L gentamicin to rapidly replicating *E. coli* in rich media, very similar to the conditions used this work, ROS could only be detected after two hours of drug treatment[30]. In a related study, the same group observed DNA damage as early as 30 minutes following treatment with 3 mg/L kanamycin treatment[31], which aligns with our findings (**Figure 2b**). Further investigations are warranted to clarify the relative contribution of these pathways at different stages of aminoglycoside treatment in determining the ultimate cellular fate.

Due to the DNA damage induced by ribosome antibiotics, the ensuing activation of SOS response and error-prone DNA repair systems introduced a substantially higher burden of mutagenesis. Our findings demonstrate the functionality of this induced mutagenesis, as evidenced by the rapid emergence of resistant mutants and their distinct mutation spectrum. Thus, at least under our experimental setup, these results offer a robust molecular-level mechanism underpinning the contentious concept of inducible evolution. Interestingly, we also observed that a subset of cells within the isogenic population exhibited hyperactivated SOS responses, resulting in greater

tolerance compared to their counterparts with normal SOS responses. We propose that this heterogeneous SOS response predisposes highly tolerant cells to induced mutagenesis, thereby facilitating accelerated evolution towards genetic resistance. In this context, the proficient DNA repair capacity ensures timely damage resolution, thereby enabling the survival of a viable cell population, which is a prior to any potential evolutionary processes. Subsequently, the potentially error-prone repair systems introduce sufficient genetic alterations to serve as the raw material for resistance evolution. This structural arrangement bears resemblance to the recently demonstrated gambling strategy employed by bacterial populations when confronted with ciprofloxacin treatment[10]. As bacterial SOS responses are inherently heterogenous[60], we speculate that such a bet-hedging program, aimed at expediting genotype scanning, could be exploited by bacteria facing a broader spectrum of acute environmental stresses. Another interesting possibility is about the role of ribosome in bacterial evolution. Serving as a signaling hub for sensing intracellular energy, nutrient availability, and stress states[25,61], our work suggested that ribosome could modulate induced mutagenesis. Depending on the alarm levels quantified by the extent of acute translational deceleration, such modulation may operate in a dose-dependent manner, thereby contributing to population survival during environmental fluctuations. Indeed, several ribosome inhibitors with sub-MIC concentrations have been reported to trigger bacterial DNA damage[62] and activate genetic diversification[27].

Our findings unveil a swift transition in survival strategies from phenotypic tolerance to genetic resistance upon exposure of rapidly growing *E. coli* to gentamicin. In this specific context, the role of persistence[1] is minimal. It is well-established that persistence aids bacterial survival under high drug concentrations. However, in our study, the concentration of gentamicin used (6 mg/L)

corresponds to approximately two-fold of MIC. We also note that our experimental setting mimics the pharmacokinetics of gentamicin in human serum, where averaged peak concentration ranges from 2.8 mg/L[34] to 17 mg/L[35] and averaged $t_{1/2}$ ranges from 1.2 h[34] to 5.0 h[35]. Hence, under clinically relevant conditions, the rapid emergence of de novo resistance facilitated by induced mutagenesis becomes the dominant mechanism in the later stages of bacterial survival, rendering persistence dispensable in this context. These results thus underscore the importance to consider timing when designing drug administration protocols. Initially, phenotypic tolerance is critical to eradication efficacy. However, in later stages, the decision to employ novel anti-persistence[63] or anti-evolvability[28,64] drugs should depend on the in vivo drug concentration and duration, which determine the relative importance of resistance evolution and persistence.

Bacteria possess a repertoire of transcriptional elongation factors that are involved in facilitating the functions of RNAP[65]. We found that many of them play critical roles in handling the secondary DNA damage induced by ribosome antibiotics. Notably, anti-backtracking factors Mfd, GreA, GreB were crucial for bacterial survival under gentamicin treatment via preventing DNA damage, while the pro-backtracking factor UvrD exacerbated genomic instability. In this line, UvrD, which is typically involved in normal DNA repair processes like transcription-coupled repair (TCR), is hijacked by ribosome antibiotics to instigate severe DNA damage. Interestingly, Sivaramakrishnan et al. recently reported that anti-backtracking factor GreA impeded DNA break repair[66], seemingly contrasting our findings. We propose that this disparity arises from distinct stress conditions used in these two studies. Sivaramakrishnan et al. directly induced DNA damage using genotoxic agents, wherein the primary objective of cells is to repair the DNA lesion. Anti-backtracking proteins then hinder the access of repair machinery to the lesion sites. By contrast, we used proteotoxic stresses,

where DNA damage is indirectly caused by TTC disruption and subsequent PRSEs. Here, the paramount concern is not to repair the DNA (although damage does occur), but the rescue of stalled RNAPs, which triggers DNA damage. Thus, while genomic instability serves as the common path leading to cellular demise in both scenarios, the relative importance of repair versus prevention of such damage differs depending on the specific stress encountered by bacteria. Manipulating transcription by targeting specific elongation factors represents a promising but underexplored avenue to enhance the efficacy of both genotoxic and proteotoxic antimicrobial agents, as it occupies an intermediate step in the central dogma.

In this work, we focused on the functional consequences of TTC disruption and PRSEs towards DNA damage. However, genome-wide PRSEs also impact functional gene expressions. Specifically, pronounced PRSEs result in a reduction in the abundance of fully transcribed functional transcripts encompassing the entire CDS, which act as a hinderance to the upregulation of critical pathways necessary for combating antibiotics. Interestingly, we observed distinct PRSE profiles across different genes, with some genes displaying insensitivity to PRSE generation while others were prone to PRSEs. These findings indicate an additional, often overlooked, systems-level factor that contributes to the efficacy of ribosome antibiotics—the impact on the expression of stress response genes mediated by PRSEs. Exploring this factor could provide insights into longstanding questions in microbiology, such as the variability in clearance efficacy observed among different ribosome antibiotics.

References

1. Brauner, A., Fridman, O., Gefen, O. & Balaban, N. Q. Distinguishing between resistance, tolerance and persistence to antibiotic treatment. *Nat. Rev. Microbiol.* **14**, 320–330 (2016).

2. Andersson, D. I. *et al.* Antibiotic resistance: Turning evolutionary principles into clinical reality. *FEMS Microbiol. Rev.* **44**, 171–188 (2020).

3. Liu, J., Gefen, O., Ronin, I., Bar-Meir, M. & Balaban, N. Q. Effect of tolerance on the evolution of antibiotic resistance under drug combinations. *Science* **367**, 200–204 (2020).

4. Stracy, M. *et al.* Minimizing treatment-induced emergence of antibiotic resistance in bacterial infections. *Science (80-.).* **894**, 889–894 (2022).

5. Murray, C. J. *et al.* Global burden of bacterial antimicrobial resistance in 2019: a systematic analysis. *Lancet* **399**, 629–655 (2020).

6. Miethke, M. *et al.* Towards the sustainable discovery and development of new antibiotics. *Nat. Rev. Chem.* **5**, 726–749 (2021).

7. Zampieri, M., Zimmermann, M., Claassen, M. & Sauer, U. Nontargeted Metabolomics Reveals the Multilevel Response to Antibiotic Perturbations. *Cell Rep.* **19**, 1214–1228 (2017).

8. Pu, Y. *et al.* ATP-Dependent Dynamic Protein Aggregation Regulates Bacterial Dormancy Depth Critical for Antibiotic Tolerance. *Mol. Cell* **73**, 143-156.e4 (2019).

9. Kohanski, M. A., Dwyer, D. J., Hayete, B., Lawrence, C. A. & Collins, J. J. A Common Mechanism of Cellular Death Induced by Bactericidal Antibiotics. *Cell* **130**, 797–810 (2007).

10. Pribis, J. P. *et al.* Gamblers: An Antibiotic-Induced Evolvable Cell Subpopulation Differentiated by Reactive-Oxygen-Induced General Stress Response. *Mol. Cell* **74**, 785-800.e7 (2019).

11. Bruni, G. N. & Kralj, J. M. Membrane voltage dysregulation driven by metabolic dysfunction underlies bactericidal activity of aminoglycosides. *Elife* **9**, e58706 (2020).

12. Baquero, F. & Levin, B. R. Proximate and ultimate causes of the bactericidal action of antibiotics. *Nat. Rev. Microbiol.* **19**, 123–132 (2021).

13. Salamaga, B. *et al.* Demonstration of the role of cell wall homeostasis in Staphylococcus aureus growth and the action of bactericidal antibiotics. *Proc. Natl. Acad. Sci. U. S. A.* **118**, 1–8 (2021).

14. Wang, C. *et al.* Structural basis of transcription-translation coupling. *Science (80-.).* **1365**, 1359–1365 (2020).

15. O'Reilly, F. J. *et al.* In-cell architecture of an actively transcribing-translating expressome. *Science (80-.).* **369**, 554–557 (2020).

16. Kang, J. Y. *et al.* Structural basis for transcription complex disruption by the mfd translocase. *Elife* **10**, e62117 (2021).

17. Blaha, G. M. & Wade, J. T. Transcription-Translation Coupling in Bacteria. *Annu. Rev. Genet.* **56**, 187–205 (2022).

18. Merrikh, H., Zhang, Y., Grossman, A. D. & Wang, J. D. Replication-transcription conflicts in bacteria. *Nat. Rev. Microbiol.* **10**, 449–458 (2012).

19. Kamarthapu, V. *et al.* ppGpp couples transcription to DNA repair in E. coli. *Science*

(80-.). **352**, 1–5 (2016).

20. Johnson, G. E., Lalanne, J. B., Peters, M. L. & Li, G. W. Functionally uncoupled transcription–translation in Bacillus subtilis. *Nature* **585**, (2020).

21. Proshkin, S., Rachid Rahmouni, A., Mironov, A. & Nudler, E. Cooperation between translating ribosomes and RNA polymerase in transcription elongation. *Science (80-.).* **328**, 5977 (2010).

22. Zhu, M., Mori, M., Hwa, T. & Dai, X. Disruption of transcription–translation coordination in Escherichia coli leads to premature transcriptional termination. *Nat. Microbiol.* **4**, 2347–2356 (2019).

23. Wee, L. M. *et al.* A trailing ribosome speeds up RNA polymerase at the expense of transcript fidelity via force and allostery. *Cell* **186**, 1244–1262 (2023).

24. Bharati, B. K. *et al.* Crucial role and mechanism of transcription-coupled DNA repair in bacteria. *Nature* **604**, 152–159 (2022).

25. Dutta, D., Shatalin, K., Epshtein, V., Gottesman, M. E. & Nudler, E. Linking RNA polymerase backtracking to genome instability in E. coli. *Cell* **146**, 533–543 (2011).

26. Sankar, T. S., Wastuwidyaningtyas, B. D., Dong, Y., Lewis, S. A. & Wang, J. D. The nature of mutations induced by replication-transcription collisions. *Nature* **535**, 178–181 (2016).

27. Blázquez, J., Rodríguez-Beltrán, J. & Matic, I. Antibiotic-Induced Genetic Variation: How It Arises and How It Can Be Prevented. *Annu. Rev. Microbiol.* **72**, 209–230 (2018).

28. Pribis, J. P., Zhai, Y., Hastings, P. J. & Rosenberg, M. Stress-Induced Mutagenesis,

Gambler Cells, and Stealth Targeting Antibiotic-Induced Evolution. *MBio* **13**, mbio.01074-22 (2022).

29. Lin, J., Zhou, D., Steitz, T. A., Polikanov, Y. S. & Gagnon, M. G. Ribosome-Targeting Antibiotics: Modes of Action, Mechanisms of Resistance, and Implications for Drug Design. *Annu. Rev. Biochem.* **87**, 451–478 (2018).

30. Kohanski, M. A., Dwyer, D. J., Wierzbowski, J., Cottarel, G. & Collins, J. J. Mistranslation of Membrane Proteins and Two-Component System Activation Trigger Antibiotic-Mediated Cell Death. *Cell* **135**, 679–690 (2008).

31. Foti, J. J., Devadoss, B., Winkler, J., Collins, J. & Walker, G. Oxidation of the Guanine Nucleotide Pool Underlies Cell Death by Bactericidal Antibiotics. *Science (80-.).* **336**, 315–319 (2012).

32. Levin, B. R. *et al.* A Numbers Game: Ribosome Densities, Bacterial Growth, and Antibiotic- Mediated Stasis and Death. *MBio* **8**, e02253-16 (2017).

33. Serio, A. W., Keepers, T., Andrews, L. & Krause, K. M. Aminoglycoside Revival: Review of a Historically Important Class of Antimicrobials Undergoing Rejuvenation. *EcoSal Plus* **8**, (2018).

34. Siber, G. R., Echeverria, P., Smith, A. L., Paisley, J. W. & Smith, D. H. Pharmacokinetics of gentamicin in children and adults. *J. Infect. Dis.* **132**, 637–651 (1975).

35. Gonçalves-Pereira, J., Martins, A. & Póvoa, P. Pharmacokinetics of gentamicin in critically ill patients: Pilot study evaluating the first dose. *Clin. Microbiol. Infect.* **16**, 1258–1263 (2010).

36. Yu, J. S. L. *et al.* Microbial communities form rich extracellular metabolomes that foster metabolic interactions and promote drug tolerance. *Nat. Microbiol.* **7**, 542–555 (2022).

37. Levin-Reisman, I. *et al.* Antibiotic tolerance facilitates the evolution of resistance. *Science* **355**, 826–830 (2017).

38. Ibacache-Quiroga, C., Oliveros, J. C., Couce, A. & Blázquez, J. Parallel evolution of high-level aminoglycoside resistance in Escherichia coli under low and high mutation supply rates. *Front. Microbiol.* **9**, 427 (2018).

39. Girgis, H. S., Hottes, A. K. & Tavazoie, S. Genetic architecture of intrinsic antibiotic susceptibility. *PLoS One* **4**, e5629 (2009).

40. Maslowska, K. H., Makiela-Dzbenska, K. & Fijalkowska, I. J. The SOS system: A complex and tightly regulated response to DNA damage. *Environ. Mol. Mutagen.* **60**, 368–384 (2019).

41. Guerin, É. *et al.* The SOS Response Controls Integron Recombination. *Science (80-.).* **324**, 1034 (2009).

42. Wagner, J. & Nohmi, T. Escherichia coli DNA polymerase IV mutator activity: Genetic requirements and mutational specificity. *J. Bacteriol.* **182**, 4587–4595 (2000).

43. Niccum, B. A. *et al.* New complexities of SOS-induced "untargeted" mutagenesis in Escherichia coli as revealed by mutation accumulation and whole-genome sequencing. *DNA Repair (Amst).* **90**, 102852 (2020).

44. Gowrishankar, J., Krishna Leela, J. & Anupama, K. R-loops in bacterial transcription: Their causes and consequences. *Transcription* **4**, 153–157 (2013).

45. Drolet, M. & Brochu, J. R-loop-dependent replication and genomic instability in bacteria. *DNA Repair (Amst).* **84**, 102693 (2019).

46. Ragheb, M. N., Merrikh, C., Browning, K. & Merrikh, H. Mfd regulates RNA polymerase association with hard-to-transcribe regions in vivo, especially those with structured RNAs. *Proc. Natl. Acad. Sci. U. S. A.* **118**, e2008498118 (2020).

47. Ramirez, P., Crouch, R. J., Cheung, V. G. & Grunseich, C. R-loop analysis by dot-blot. *J. Vis. Exp.* **167**, e62069 (2021).

48. Leela, J. K., Syeda, A. H., Anupama, K. & Gowrishankar, J. Rho-dependent transcription termination is essential to prevent excessive genome-wide R-loops in Escherichia coli. *Proc. Natl. Acad. Sci. U. S. A.* **110**, 258–263 (2013).

49. Whinn, K. S., van Oijen, A. M. & Ghodke, H. Single-molecule studies of helicases and translocases in prokaryotic genome-maintenance pathways. *DNA Repair (Amst).* **108**, 103229 (2021).

50. Le, T. T. *et al.* Mfd Dynamically Regulates Transcription via a Release and Catch-Up Mechanism. *Cell* **172**, 344-357.e15 (2018).

51. Lindsey-Boltz, L. A. & Sancar, A. The Transcription-Repair Coupling Factor Mfd Prevents and Promotes Mutagenesis in a Context-Dependent Manner. *Front. Mol. Biosci.* **8**, 668290 (2021).

52. Epshtein, V. *et al.* UvrD facilitates DNA repair by pulling RNA polymerase backwards. *Nature* **505**, 372–377 (2014).

53. Le, T. T. & Wang, M. D. Molecular Highways—Navigating Collisions of DNA Motor

Proteins. *J. Mol. Biol.* **430**, 4513–4524 (2018).

54. Wang, T. *et al.* Dynamics of transcription–translation coordination tune bacterial indole signaling. *Nat. Chem. Biol.* **16**, 440–449 (2020).

55. Artsimovitch, I. & Landick, R. Interaction of a nascent RNA structure with RNA polymerase is required for hairpin-dependent transcriptional pausing but not for transcript release. *Genes Dev.* **12**, 3110–3122 (1998).

56. Chong, S., Chen, C., Ge, H. & Xie, X. S. Mechanism of transcriptional bursting in bacteria. *Cell* **158**, 314–326 (2014).

57. Kohanski, M. A., Dwyer, D. J. & Collins, J. J. How antibiotics kill bacteria: from targets to networks. *Nat. Rev. Microbiol.* **8**, 423–435 (2010).

58. Kaplan, Y. *et al.* Observation of universal ageing dynamics in antibiotic persistence. *Nature* **600**, 290–294 (2021).

59. Shaffer, S. M. *et al.* Rare cell variability and drug-induced reprogramming as a mode of cancer drug resistance. *Nature* **546**, 431–435 (2017).

60. Jones, E. C. & Uphoff, S. Single-molecule imaging of LexA degradation in Escherichia coli elucidates regulatory mechanisms and heterogeneity of the SOS response. *Nat. Microbiol.* **6**, 981–990 (2021).

61. Li, S. H.-J. *et al.* Escherichia coli translation strategies differ across carbon, nitrogen and phosphorus limitation conditions. *Nat. Microbiol.* **3**, 939–947 (2018).

62. Negro, V. *et al.* RadD Contributes to R-Loop Avoidance in Sub-MIC Tobramycin. *MBio* **10**, e01173-19 (2019).

63. Lázár, V., Snitser, O., Barkan, D. & Kishony, R. Antibiotic combinations reduce Staphylococcus aureus clearance. *Nature* **610**, 540–546 (2022).

64. Balbontín, R., Frazão, N. & Gordo, I. DNA Breaks-Mediated Fitness Cost Reveals RNase HI as a New Target for Selectively Eliminating Antibiotic-Resistant Bacteria. *Mol. Biol. Evol.* **38**, 3220–3234 (2021).

65. Borukhov, S., Lee, J. & Laptenko, O. Bacterial transcription elongation factors: New insights into molecular mechanism of action. *Mol. Microbiol.* **55**, 1315–1324 (2005).

66. Sivaramakrishnan, P. *et al.* The transcription fidelity factor GreA impedes DNA break repair. *Nature* **550**, 214–218 (2017).

67. Baba, T. *et al.* Construction of Escherichia coli K-12 in-frame, single-gene knockout mutants: the Keio collection. *Mol. Syst. Biol.* **2**, 2006.0008 (2006).

68. Datsenko, K. A. & Wanner, B. L. One-step inactivation of chromosomal genes in Escherichia coli K-12 using PCR products. *Proc. Natl. Acad. Sci. U. S. A.* **97**, 6640–6645 (2000).

69. Jiang, Y. *et al.* Multigene editing in the Escherichia coli genome using the CRISPR-Cas9 system. *Appl. Environ. Microbiol.* **81**, 2506–14 (2015).

70. Wang, T., Shen, P., He, Y., Zhang, Y. & Liu, J. Spatial transcriptome uncovers rich coordination of metabolism in E. coli K12 biofilm. *Nat. Chem. Biol.* (2023). doi:10.1038/s41589-023-01282-w

71. Wang, T. *et al.* Pooled CRISPR interference screening enables genome-scale functional genomics study in bacteria with superior performance. *Nat. Commun.* **9**, 2475 (2018).

72. Chen, X. *et al.* Visualizing RNA dynamics in live cells with bright and stable fluorescent RNAs. *Nat. Biotechnol.* **37**, 1287–1293 (2019).

73. Wu, J., Dai, W., Wu, L. & Wang, J. SALP, a new single-stranded DNA library preparation method especially useful for the high-throughput characterization of chromatin openness states. *BMC Genomics* **19**, 143 (2018).

74. Deatherage, D. E. & Barrick, J. E. Identification of mutations in laboratory-evolved microbes from next-generation sequencing data using breseq. *Methods Mol. Biol.* **1151**, 165–188 (2014).

75. Gunderson, K. & Chu, G. Pulsed-Field Electrophoresis of Megabase-Sized DNA. *Mol. Cell. Biol.* **11**, 3348–54 (1991).

76. Avraham, R. *et al.* A highly multiplexed and sensitive RNA-seq protocol for simultaneous analysis of host and pathogen transcriptomes. *Nat. Protoc.* **11**, 1477–1491 (2016).

77. Wang, T., Shen, P., Chai, R., He, Y. & Liu, J. Profiling of bacterial transcriptome from ultra-low input with MiniBac-seq. *Environ. Microbiol.* **24**, 5774–5787 (2022).

78. Kerpedjiev, P., Hammer, S. & Hofacker, I. L. Forna (force-directed RNA): Simple and effective online RNA secondary structure diagrams. *Bioinformatics* **31**, 3377–3379 (2015).

Methods

Bacterial strains and cultivation conditions

In all experiments, *E. coli* K12 BW25113 was used (originally from CICC, 23872) as the wildtype strain. Single colony was picked up from a stock LB agar plate and was grown aerobically with shaking at 220 rpm in Luria-Bertani (LB) broth (10 g/L tryptone (Oxoid, LP0042), 10 g/L NaCl (Macklin, S805275), 5 g/L yeast extract (Oxoid, LP0021)) medium overnight (typically 12 h) as the seed culture. All cultures were carried out at 37 °C with shaking at 220 rpm. When necessary, 100 mg/L ampicillin (TargetMol, T6386) was supplemented to maintain the plasmid. All knockout strains were derived from Keio collection. The excision of FRT-flanked *kan* cassette in Keio knockout strains[67] was carried out by FLP recombinase-expressing pCP20 plasmid[68]; PCRs with specific primers towards the deleted loci were adopted to confirm knockout and *kan* cassette excision. The *kan*-free knockout strains were then used in our experiments. Besides knockout strains from Keio collection, the *tolC* F16* (TTC→TGA) strain was an *E. coli* K12 BW25113 derivate constructed by CRISPR genome editing[69], where a premature stop codon was introduced into the chromosome to attenuate the efflux function of TolC pump. *E. coli* strain DH10B (BioMed) was used as host during molecular cloning to construct plasmids.

Plasmid construction

The construction of the P_{recA}_*pepper* plasmid used to surveil SOS responses was described below. We first adopted PCR to amplify *recA* promoter from *E. coli* K12 BW25113 genomic DNA, p15A plasmid origin of replication from p15A_*PpyrLBI*_mCherry[70], ampicillin resistance cassette from pTargetF_lac[71], giving rise to three DNA fragments. We also purchased a synthetic pepper

construct consisted of four repeated HBC620 binding motif sequences from GENEWIZ Int. Co., which was designed according to the nucleotide sequence reported by Chen et al.[72]. Starting from these four DNA fragments, we constructed P_{recA}_*pepper* plasmid via assembling them with each other by Gibson assembly. The nucleotide sequence of the constructed plasmid was confirmed by Sanger sequencing and deposited at benchling (https://benchling.com/s/seq-oujd4XqzHbQnUPkf85hy?m=slm-nDZVa3rRVTOgNMWLIMQW).

Drug treatment

In most cases, overnight seed cultures were diluted by 1:350 into 700 μL of fresh medium and grown in a 48-well plate in a microplate reader (Tecan, Spark). When the cultures grew to OD_{600} ~ 0.2, we carried out another dilution of 1:50 into fresh medium and cultivated with the same condition. When subcultures reached an OD_{600} of ~ 0.25, 10 μL gentamicin (Selleck, S4030) was supplemented to make a final concentration of 6 mg/L. Sometimes when gentamicin treatments were needed for many mutants, we adopted a 96-well plate to perform these experiments, while keeping all other settings the same as described above.

Similar protocols were adopted to treat bacterial cultures by other ribosome antibiotics with the following concentrations (**Figure 6b**). Gentamicin (Selleck, S4030), 2.5, 5, 10, 20, 40 mg/L; Chloramphenicol (Solarbio, C8050), 11.7, 23.4, 46.9, 93.8, 187.5 mg/L; Lincomycin (TargetMol, T1277), 390.6, 781.3, 1562.5, 3125, 6250 mg/L; Puromycin (Macklin, P816466), 97.7, 195.3, 390.6, 781.3, 1562.5 mg/L; Azithromycin (Selleck, S1835), 7.8, 15.6, 31.3, 62.5, 125 mg/L; Solithromycin (Selleck, S5268), 7.8, 15.6, 31.3, 62.5, 125 mg/L; Streptomycin (inalco, 1758-9319),

14.6, 29.3, 58.6, 117.2, 234.4 mg/L; Spectinomycin (Macklin, S6106), 39.1, 78.1, 156.3, 312.5, 625 mg/L; Tigecycline (Macklin, T830543), 1, 2, 4, 8, 16 mg/L; Fusidic acid sodium (Macklin, F860722), 195.3, 390.6, 781.3, 1562.5, 3125 mg/L; Tetracycline (Solarbio, ST8750), 1.25, 2.5, 5, 10, 20 mg/L.

Throughout the cultivation, OD_{600} was monitored every 10 min so as to add drugs and to surveil and to surveil growth curve.

Killing assay to determine drug lethality

At specific time points after drug (gentamicin) treatment, aliquots of 100 μL culture were taken from the corresponding well in microplate readers; We only performed one sampling from each well. Bacteria in the culture were immediately pelleted by centrifugation at 5,000 *g* for 2 min. Pellets was resuspended with fresh medium and properly diluted, then plated onto LB agar plates containing no antibiotics. The plates were incubated at 37 °C for 48 hours before determination of colony-forming units (CFU). When necessary, we recovered colonies here as isolated survivors for other experiments, including drug susceptibility assay and genome resequencing (discussed below).

Drug susceptibility assay by AUC of bacterial growth

We adopted a drug susceptibility assay[36] as a sensitive and high-throughput method to identify the survival modes (see below) upon drug treatment, specified as below. Strains to be tested were

randomly picked among survived clones from agar plates in killing assay. Their overnight seed cultures were diluted 1:350 into 700 μL of fresh medium and grown in 48-well plate in a microplate reader (Tecan Spark). When cultures grew to OD_{600} ~ 0.2, they were diluted 1:15 into wells of 96-well plate containing gentamicin of 0 mg/L, 2 mg/L, 3 mg/L, 4 mg/L, 6 mg/L, 8 mg/L, respectively. Cultivation was carried in the microplate reader (Tecan, Spark) for 20 hours, during which OD_{600} was monitored every 30 min. The AUC of the growth curve for each strain under drug treatment of particular concentration was next calculated; And the AUC profile was used to quantify the drug susceptibility.

Definitions of different survival modes

Four survival modes are mentioned in this work (**Figure 1d**), here we presented their strict definitions. We referred to the three terms, phenotypic persistence, genotypic tolerance and genotypic resistance, basically according to the description by Brauner et al.[1]. In particular, phenotypic persistence is the ability of a subset of bacterial population which exhibits lower killing rate than the majority of this population when exposing to a bactericidal drug concentration. Phenotypic persistence is hallmarked by the second phase of the biphasic killing curve. As a result, phenotypic persistence is a phenomenon related to single-cell heterogeneity and therefore genetically non-heritable. By contrast, the first phase of the killing curve, suggests that the majority of cells in this population is being killed by a constant rate (faster than the persister subpopulation); And some cells survives longer than others in this phase, which we called phenotypic tolerance. Hence, phenotypic tolerance also derives from the heterogeneity at single cell level.

In contrast, genotypic tolerance suggests that some mutations in the genome lead to better survival of the whole population when exposing to a bactericidal drug concentration, which is reflected by a slower killing rate in the (first phase of) killing curve. As its definition, genotypic tolerance is genetically inheritable. Reisman et al. elegantly showed that prolonged lag time in the absence of drugs acted as a hallmark of genotypic tolerance[37]. Similarly, genotypic resistance suggests that some mutations lead to bacterial growth under drug concentrations that originally completely inhibit the replication of the wildtype strain. Genotypic resistance is hallmarked by an increase in MIC and genetically inheritable.

According to these definitions and our drug susceptibility assay results (**Figure 1d**), we concluded that phenotypic tolerance dominated bacterial survival before 90 min gentamicin treatment. Phenotypic persistence, that enhanced subpopulation survival after prolonged drug treatment, was irrelevant in our scenario, since mutations leading to genotypic tolerance and resistance rapidly emerged. We also categorized those mutants with increased resistance (bigger AUC_x, x= 2 or 3 or 4 or 6 or 8) as genotypic resistance. In contrast, the remaining mutants, which exhibited extended lag time in the absence of gentamicin (smaller AUC_0) and similar growth under drug treatment when compared with wildtype (similar AUC_x, x = 2, 3, 4, 6, 8), were categorized to genotypic tolerance.

TUNEL assay to quantify DNA damage

The chemistry of TUNEL assay was described in **Supplementary Figure 2a**. At specific time points after gentamicin treatment, aliquots of 100 μL culture were taken from culture. Bacteria

were collected by centrifugation at 1,000 *g* for 2 min and washed once with 0.2 mL PBS. The bacteria were then fixed with 0.8 mL 3% PFA (Sigma-Aldrich, F8775) and gently rotated for 15 min at room temperature. After fixation, samples were pelleted by centrifugation at 2,000 *g* for 2 min and washed twice with 1 mL PBS, then permeabilized with 0.5 mL 70% ethanol (Sigma-Aldrich, 459844) in -20 °C overnight. Next day, permeabilized bacteria samples were pelleted by centrifugation at 2,000 *g* for 2 min and washed twice with 1 mL water.

Labelling for DNA lesion was performed using the Click-iT TUNEL Alexa Fluor 488 kit (Thermo Fisher, C10245). For the TdT reaction, the pellets were resuspended with 50 μL systems, containing 1 μL EdUTP and 2 μL TdT in 1×TdT reaction buffer. Then the reaction systems were incubated at 37 °C for 30 min. When the reactions finished, pellets were again collected by centrifugation at 2,000 *g* for 2 min, and were washed once with 0.1 mL water. Next, the Click-iT reactions were performed by incubating in 100 μL systems, consisted of 2.5 μL additive in 1×Click-iT reaction buffer, at room temperature for 30 min, protected from light. After the reaction cells were pelleted at 2,000 *g* for 2 min and washed once with 0.2 mL PBS. As a negative control, we skipped the TdT reaction step (**Supplementary Figure 2b**).

Finally, labeled samples were resuspended in 0.5 mL PBS and analyzed by flow cytometry (BD, Aria II SORP). Propidium iodide staining (Invitrogen, P1304MP, 1 μg/mL supplemented prior to flow cytometry) was performed before flow cytometry analysis to quantify cell permeabilization. The optical setting of the machine was described as below. FITC (for DNA lesion signals labeled by click chemistry), 488 nm blue laser, plus a 505 nm long pass filter and a 530/30 nm band-pass

filter; PE-Texas Red channel (for PI staining), a 561 nm green-to-yellow laser, plus a 600 nm long pass filter and a 610/20 nm band-pass filter. Empirically, we gated populations showing PI signal (PE-Texas Red channel) above 10^3 (AU) for the analysis of DNA lesion profile (FITC channel).

Slot-blot hybridization analysis of RNA:DNA hybrids (R-loops)

Genomic DNAs of bacteria from 2.5 mL culture after different durations of gentamicin treatment were extracted with MasterPure Complete DNA/RNA Purification Kit (LGC (Lucigen), MC85200), and their concentrations were measured by Qubit 1xdsDNA HS Assay Kit (Invitrogen, Q33230). For each sample, 10 μg DNA was treated with 2 U ShortCut RNase III (NEB, M0245S) in 100 μL reaction system at 37 °C overnight, then purified with the abovementioned MasterPure Purification Kit again. After digestion, 1 μg DNA were slotted onto Hybond N+ membrane (RPN303B, GE Healthcare). The membrane was cross-linked twice with 1,200 μJ UV light. Following UV crosslinking, the membrane was blocked in 5% milk/TBS-Tween (0.05% Tween20) at room temperature for one hour, and incubated at 4 °C overnight with anti-DNA:RNA hybrid S9.6 antibody (1:1000 dilution, abcam, ab234957). After 10-min washing in TBS-Tween (0.05% Tween20) for three times, the membrane was incubated for one hour at room temperature with HRP Goat Anti-Mouse IgG (1:5000 dilution, abclonal, AS003). Next, the membrane was washed by TBS-Tween (0.05% Tween20) for additionally three times and then developed with enhanced chemiluminescence substrate (BE6706, Easybio) for Western Blotting. S9.6 signals were detected by ImageQuant LAS 4000 (GE Healthcare).

FACS to separate bacterial subpopulations with different SOS responses

To monitor the SOS responses, we constructed a P_{recA}_*pepper* plasmid (see "Plasmid construction" subsection in **Methods**), which surveilled the promoter activity of *recA*, the master regulator of SOS responses with positive feedback autoregulation via triggering LexA transcriptional repressor self-cleavage[40]. Additionally, to bypass the impact of translation inhibition on the expression of reporter gene, instead of typically used fluorescent proteins, we exploited a fluorescent RNA, named after *pepper*, which allowed simple and robust imaging of RNA species in living cells[72]. In particular, a small molecule HBC620 (TargetMol, T19352) entered cells and only became fluorescent when forming complex with *pepper* RNAs[72]. Here, note that to maximize the sensitivity of this reporter, we used an *E. coli* K12 BW25113 strain with a dysfunctional efflux pump TolC, as the host in this assay (for the construction of this strain, see "Bacterial strains and cultivation conditions" subsection in **Methods**); This strain allowed enhanced accumulation of intracellular free HBC620 and thus maximized reporter signals. These designs are essential to quantify SOS responses with high signal-to-noise ratio and at singlecell resolution in our experimental setting (translation inhibition), as we actually comprehensively tested many genetically encoded reporter systems. We transformed P_{recA}_*pepper* reporter plasmid into this host strain with dysfunctional TolC, which was regarded as the SOS reporter strain hereafter. Ampicillin was always supplemented to medium and agar plate mentioned below to maintain the plasmid in the SOS reporter strain. We experimentally confirmed that both externally added HBC620 and endogenously expressed *pepper* RNA were essential to the fluorescence signal, consistent with the report by Chen et al.[72].

The drug treatment of this SOS reporter strain was similar to the regular steps (see "Drug treatment" subsection in **Methods**), except that 5 μM HBC620 was added to the medium during the second

subculture. After gentamicin treatment for 40 min, 50 μL culture was diluted in 950 μL PBS for FACS. Non-cell particles were excluded via FSC-SSC gating. Cells were analyzed for their SOS responses in the PE-Texas Red channel (for optical setting, see "TUNEL assay" subsection in **Methods**). Among whole population, the 5% of cells with strongest signals were gated as SOS-high group, while the ones ranked bottom 40% were assigned as SOS-low. For each group, 50,000 cells were sorted in a four-way setting and collected into 1.5 mL EP-tube containing 0.5 mL LB medium. After recovery in shaker for 20 min at 37 °C, all cultures were plated onto LB agar in 6-well plates, and incubated at 37 °C for 24 hours before CFU counting; The survival rate of each group was next calculated by dividing the corresponding (survived) CFU count by 50,000, the original number of cells collected during FACS. We also showed that without gentamicin treatment, the SOS-high and SOS-low groups exhibited comparable 100% survival rates after cell sorting (**Figure 6e**), suggesting that sorting process did not introduce cell damages or group-wise biases in this assay.

Genome re-sequencing

After library construction according to standard protocol, we subjected the samples to sequencing by Novogene Bioinformatics Institute via Illumina NovaSeq 6000 system with 2×150 pair-end configuration. Typically, we got three million pair-end reads for each sample, corresponding to ~50-fold genome coverage. After demultiplexing, we trimmed adaptor sequences by cutadapt (v0.11.9) and adopted breseq (0.35.3)[74] to identify mutations from the first read of the NGS data in a default clonal mode against the reference genome (NC000913.3). Those identified mutations carried by our wildtype strain were regarded as spontaneous mutations. Note that we excluded mutations derived from genetic manipulations during the construction history of *E. coli* K12

MG1655, such as deletions of several sugar utilization operons[67]. Except for spontaneous mutations, any other genetic alternation identified in the survived isolates was regarded as mutations emerged during seed culture or gentamicin treatment, which was subjected to mutation spectrum analysis.

Pulse-field gel electrophoresis

We adopted the protocol as described previously[75]. Around 10^8 *E. coli* cells were collected at a series of time points after gentamicin treatment from 48-well plate. After pelleted by soft spin of 700 *g* for 2 min (to minimize DNA damage introduced by centrifugation), bacteria were resuspended by 100 μL LB and 1:1 thoroughly mixed with 2% low melting point agarose (Promega, V2111) preheated to 42 °C, and then molded into plugs. When solidified, the agarose plugs were treated with lysozyme for two hours at 37 °C. The lysozyme solution contained 1 mg/mL lysozyme (Sigma, 62970), 10 mM Tris pH 7.0 (Solarbio, T1130), 50 mM NaCl (Thermo Fisher, AM9760G), 0.2% sodium deoxycholate (Sigma, 30970), 0.5% sodium lauryl sarcosine (Sigma, 61745). Next, the plugs were rinsed with sterile water and were then incubated in Proteinase K solution for 12 hours at 50 °C with mild agitation. The Proteinase K solution contained 1 mg/mL Proteinase K (Sigma, 539480), 100 mM EDTA (Solarbio, E1170), 0.2% sodium deoxycholate, 1% sodium lauryl sarcosine. After digestion, the plugs were washed for six times (10 min each with mild agitation) in wash buffer, containing 20 mM Tris pH 8.0 (Solarbio, T1150), 50 mM EDTA. The plugs were inserted into wells of 1% agarose gel in 0.5× TBE (huaxingbio, HX1872) and sealed by agarose solution. Genomic DNA fragments were then separated by BioRad CHEF Mapper® pulsed-field electrophoresis system. Running conditions were generated by the Auto-Algorithm mode using a size range of 1-100 kb: 0.5× TBE at 14 °C for 07:53 hours at 6.0 V/cm using a 120°

included angle with a 0.06-8.53 second linear switch time ramp. Gels were stained with Genecolor I (Gene-bio, GBY-1) and visualized with UV-trans-illumination. The intensity of DNA bands was quantified using ImageJ software.

Total RNA extraction

The bacteria cultivation and drug treatment were as described above. At specific time points before or after drug treatment, total RNA was extracted as below. 150 uL culture was first mixed with 150 uL RNAlater (Thermo Fisher, AM7020) and set at room temperature for at least 15 min. Then, the sample was diluted with 600 uL ice-cold PBS (SolarBio, pH 7.4, P1020-500) and centrifuged with 5,000g for 15 min. After discarding the supernatant, the cell pellet was resuspended by 50 uL of TE buffer (10 mM Tris, 1 mM disodium EDTA, pH = 8.0, Thermo Fisher, AM9849) containing 12.5 mg/ml of lysozyme (SIGMA, 62970-1G-F) and 16.7% (v:v) proteinase K (QIAGEN, 19131) to lyse cells. The mixture was incubated at 37 ℃ for 15 min and subjected to purification; Here 100 uL of RNACleanXP beads (Beckman, A63987) was mixed with lysate and incubated at room temperature for 15 min; placed on a magnet for 10 min. Then, the supernatant was discarded. The beads were washed twice by 200 uL 80% (v:v) ethanol (SIGMA, 459844-500Ml) and air-dried for 15 min on the magnet rack. Finally, the beads were resuspended by 21 uL nuclease free water; set at room temperature for 15 min; put back on magnet; let stand for 5 min. Finally, the supernatant was transferred to a new tube, giving rise to the purified total RNA. Concentration of total RNA was measured by Qubit (Thermo Fisher, Q32855) and stored at -80 ℃ before usage.

3'-end-seq and RNA-seq library construction

For each purified sample, total RNA was subjected to 3'-end-seq and RNA-seq library preparation respectively.

The 3'-end-seq library preparation method was adopted from a previous multiplexed RNA-seq library preparation method reported by Avraham et al.[76]. Systematic modifications were introduced to repurpose it to keep 3' end information of bacterial transcripts. First, without any fragmentation, 100 ng total RNA was dephosphorylated by FastAP (Thermo Fisher, EF0651) and depleted of genomic DNA by Turbo DNase (Thermo Fisher, AM2238). Then, RNA adaptors ((5'Phos/NNNNNNNNNAGAUCGGAAGAGCGUCGUGUA/3'SpC3, synthesized by GenScript and purified by RNase free HPLC) were ligated to 3' ends of total bacterial RNA by T4 RNA ligase I (NEB, M0437M). Each RNA adaptor carried a 5' phosphate, a 3' C3 blocking group, a 3' constant sequence containing i5 adaptor sequence and also used in reverse transcription, a unique 5' barcode for multiplexing. Next, four to five 3' ligated RNA samples were pooled together and purified by RNeasy column (QIAGEN, 74104). Purified RNA was subjected to an RNaseH-based (NEB, M0523S) reaction to deplete rRNA plus noncoding element *ssrA* as previously described[77]. RNA was purified by RNAClean XP beads with two rounds 100% ethanol washing and then converted to double strand cDNA (dsDNA) by reverse transcription (NEB, 0466S) with a constant primer targeting the ligated adaptor, template switch (NEB, 0466S) and preamplification PCR for 8 cycles (KAPA, Roche, KK2502) with primers (5'-TACACGACGCTCTTCCGATCT-3'; 5'-AAGCAGTGGTATCAACGCAGAGT-3'). The oligonucleotides used in the template switch reaction were 5'-AAGCAGTGGTATCAACGCAGAGTACATrGrG+G-3' (Sangon, RNase free HPLC). The dsDNA was purified by Ampure beads with two around 80% ethanol wash. Finally, 2 ng purified

dsDNA was tagmented with N7 adaptor-incubating transposase (Vazyme, TD513); and finally PCR amplified for 11 cycles to a final product of around 100 ng. The final PCR step therefore led to biased sampling towards the 3' ends of bacterial transcripts and completely abandoned the 5'-end information. All oligonucleotides used in 3'-end-seq library preparation could be found at **Supplementary Table 4**. We also provided a comprehensive protocol of 3'-end-seq in **Supplementary Materials**.

To prepare RNA-seq library, here we did not follow routine RNA-seq library construction method, in order to minimize the batch effect introduced when applying different library preparation protocols. By contrast, RNA-seq libraries were prepared similar with 3'-end-seq protocol with two critical modifications as below: 100 ng total RNA of the same sample was firstly fragmented at 97 °C in FastAP (Thermo Fisher, EF0651) buffer for 3 minutes; Pre-PCR amplified double strand cDNA after template switch step was directly subjected to final PCR without tagmentation by transposases. Adopting these two modifications led to a uniform and unbiased sampling from bacterial transcripts, which was essential to RNA-seq that focused on transcript counting and coverage analysis, rather than the 3'-end-biased sampling as in 3'-end-seq library construction. All oligonucleotides used in RNA-seq library preparation were adopted from the 3'-end-seq protocol and therefore could also be found at **Supplementary Table 4**.

All libraries were sequenced by GENEWIZ Int. Co. via Illumina NovaSeq 6000 system with 2×150 pair-end configuration. About five million pair-end reads were yielded for each demultiplexed library.

NGS data processing for 3'-end-seq

Firstly, sequencing raw data was subjected to FastQC (v0.11.9) for quality control and cutadapt (2.10) for adaptor trimming. The data was then demultiplexed by cutadapt based on the unique RNA adaptors. Paired-end reads were aligned to *E. coli* reference genome (NC_000913.3) by bowtie2 (2.4.1) with parameters -X 1000 -I 18 --no-mixed --no-discordant. The mapped reads were converted to bam files by samtools (1.10). To minimize the effect of sequencing depth on further analysis, we subsampled every bam file to the equal number of 4.5 million paired-end reads. Reads were counted for bam files using R (4.0.2) method summarizeOverlaps from GenomicAlignments package (v1.26.0) in a strand specific manner, with the following options "mode = "Union", ignore.strand = FALSE, singleEnd = FALSE, preprocess.reads = invertStrand".

3'-end-seq bam files were used for 3' end mapping and counting by a customized R script. Due to the strandedness of our 3'-end-seq library preparation method, the genomic positions of the 5' ends from the first read in NGS raw data were actual 3' end positions of transcripts in vivo. Based on this principle, 3'-end-seq signals were counted with single-nucleotide resolutions and normalized by **C**ount **P**er **M**illion (CPM) of paired-end reads, which was regarded as 3' end intensity and used in further data analysis as well as visualization.

NGS data processing for RNA-seq

RNA-seq data processing was similar to our previous report[77]. Briefly, adaptor trimming, alignment to genome and gene read count table were all the same with 3'-end-seq as shown above. RNA-seq raw count was normalized by transcripts per million (TPM) as a quantification of RNA expression, then an TPM matrix over drug treatment time was derived. For expression data quality control, genes with average TPM < 5 or maximum TPM < 10 were excluded from further analysis, resulting in 3,173 genes remained (3,126 protein-coding genes plus 47 noncoding genes, **Supplementary Table 5**). Genome-wide strand-specific coverage files were also generated from RNA-seq data for each bam file by bedtools (v2.30.0) genomecov, with options –strand -/+ -d –pc, which was used in the gene expression polarity analysis (see "RNA-seq coverage normalization to show genome-wide gene expression polarity" subsection in **Methods**).

Technical definition of intrinsic terminator

Here we presented the definition of intrinsic terminators, which were excluded from PRSE analysis. Briefly, for each CDS, we identified its stop codon and extracted all 3' ends that occurred within 100 nt downstream this stop codon, as intrinsic terminator candidates. Then, we filtered these candidates by only keeping those with CPM values (> 1) and enrichment factor (> 20) of the corresponding 3' ends (see "Predominant PRSE calling" subsection in **Methods** for definition of enrichment factor). In some cases, more than two intrinsic terminator candidates were kept and they were too proximal to each other (within 10 nt); We only kept the best one by first selecting via CPM (choose the biggest) and next (if applicable) by enrichment factor (choose the biggest).

Next, the remained intrinsic terminator candidates of biological replicates were intersected with each other; Here, if candidates from different replicates were within 10 nt on the genome, we only kept the candidate from one replicate. Finally, the intersected candidates were defined as intrinsic terminators. The quality of this computational pipeline was verified by the high accuracy to capture known intrinsic terminators (**Supplementary Figure 4**). All intrinsic terminators (at 0 min of drug treatment) defined here were excluded from PRSE analysis as shown in the next subsection.

Technical definition of PRSE

After NGS data processing as described above, we obtained one CPM value of the corresponding 3' end at each nucleotide from the two stands on bacterial genome. Starting from this table, here we clarified the technical definition of PRSE (**Supplementary Figure 5**). We first extracted all 3' ends that exclusively occurred in gene-coding regions and on the same strand of the corresponding gene as PRSE candidates. Next, as bacterial genomes were very compact with genes that were proximal to or even overlapped with each other, some PRSE candidates might actually derive from the intrinsic termination events from the transcription of upstream genes on the same strand (**Supplementary Figure 5)**. We developed a computational pipeline to identify those intrinsic termination events (see the subsection above); and next eliminated them as well as other 3' ends located upstream or downstream 5 nt of each intrinsic terminator from PRSE candidates. Here we also eliminated the 3' ends flanking the intrinsic termination events, as we found that intrinsic termination events were always accompanied by some minor but substantial 3' ends in their flanking regions.

The remaining PRSE candidates after excluding those intrinsic transcription termination events were defined as PRSEs and used in the following analysis or calculation. As shown above (**Figure 2**), the PRSEs defined here were rare or very weak in the absence of ribosome stress and uniquely activated after drug treatment. In summary, we defined PRSEs as those 3' ends that exclusively occurred in the gene-coding regions with the same strandedness; And excluded those intrinsic termination events from transcription of upstream genes. We compiled a comprehensive PRSE list for all samples produced in this work (**Supplementary Table 6**).

Predominant PRSE calling

As one of the two statistics to dissect global PRSEs, here we presented the definition of predominant PRSEs. Briefly, predominantly PRSEs came from those PRSEs that passed a customized intensity cutoff. Here, we adopted enrichment factor as the customized criterion to identify predominant PRSEs. Enrichment factor defined to what extent the tested PRSE was stronger than the background noise in its flanking region (**Supplementary Figure 12**). To calculate the enrichment factor for each PRSE, we first computed the CPM average of three 3' ends, including the PRSE candidate itself and two others of nucleotides that flanked this PRSE on the same strand, which was referred as half-peak height of this PRSE. The corresponding background noise was calculated by averaging the 100 CPMs of 3'ends from the two 50-nt regions flanking the abovementioned three 3' ends. Given these two parameters, we finally calculated the enrichment factor for this PRSE via dividing its half-peak height by the associated background noise (**Supplementary Figure 12**).

After calculating enrichment factors for all PRSEs, we next set cutoff to identify those predominant PRSEs; PRSEs with enrichment factor higher than the threshold were defined as predominant PRSEs. We typically adopted 10, 15, 20, 25 and 50 as the cutoff, as shown in the main text and figure legend. Note that if more than two predominant PRSEs occurred within 10 nt, only one PRSE with the biggest CPM was kept as the predominant PRSE here. We compiled a comprehensive predominant PRSE list for all samples produced in this work (**Supplementary Table 7**).

Note that this statistic was also used in intrinsic termination identification as described above.

Calculation of PRSE intensity in each gene

As one of the two statistics to dissect global PRSEs, here we presented the calculation of PRSE intensity in each gene. PRSE intensity for one gene in 3'-end-seq was determined by two orthogonal factors, RNAP processivity and transcription level of this gene; And our focus in this work was transcription-level-independent RNAP processivity. Hence, we sought to develop a method to calculate normalized PRSE intensity, which was orthogonal to the transcription level and reflected inherent RNAP processivity upon drug treatment. To this end, our idea was to normalize original PRSE CPM values by the transcription level of the corresponding gene (TPM). Additionally, the abovementioned normalized PRSE intensity was an artificial unit. Only when comparing to a reference state, such as before drug treatment when RNAP processivity was normal, the change of normalized PRSE intensity enabled delineating the RNAP processivity deviation

from normal upon perturbation. Given these two general principles, we next presented strict calculation process to define the term, "change in normalized PRSE intensity" in each gene.

First, for one particular gene ($gene_j$), we defined a transcription level normalization factor (equation I), to control the gene expression change before and after drug treatment.

$$\text{Normalization factor}_j = \min(TPM_{j,\ treated}, TPM_{j,\ untreated}) / \max(TPM_{j,\ treated}, TPM_{j,\ untreated}) \qquad \text{(I)}$$

Next, the raw 3' end count of each PRSE ($PRSE_k$) associated with this gene was normalized by this factor (equation II); and therefore 3' end count was reset to a new level assuming the same transcription level before and after drug treatment.

$$\text{End count}_{j,\ k,\ treated}' = (\text{End count}_{j,\ k,\ treated} \times \text{Normalization factor}_i, \text{ if } TPM_{j,\ treated} == \max(TPM_{j,\ treated}, TPM_{i,\ untreated})) \text{ or } (\text{End count}_{j,\ k,\ treated}, \text{ if } TPM_{j,\ treated} == \min(TPM_{j,\ treated}, TPM_{j,\ untreated})) \qquad \text{(II)}$$

This normalization might loss some low abundance read count, due to the bottleneck effect during NGS library preparation and sequencing. To address this, we adopted a Poisson sampling simulation to mimic such bottleneck effect, so as to recover some potential loss. The end count′ from equation II was further processed by equation III, where end count′ below two read count was subjected to the Poisson sampling process.

$$\text{End count}_{j,\,k,\,treated}'' = (\text{Poisson sampling}(\lambda = \text{End count}_{j,\,k,\,treated}'),\ \text{if End count}_{j,\,k,\,treated}' \leq 2)\ \text{or}$$

$$(\text{End count}_{j,\,k,\,treated}',\ \text{if End count}_{j,\,k,\,treated}' > 2) \qquad \text{(III)}$$

After these steps, the normalized end count value was converted to CPM value to normalize the effect from sequencing depth by equation IV.

$$\text{End CPM}_{j,\,k,\,treated}'' = (\text{End count}_{j,\,k,\,treated}'' \times 10^6) \,/\, \text{total depth}_{treated} \text{ in 3'-end-seq library} \qquad \text{(IV)}$$

Finally, normalized PRSE intensity of one gene from one sample (such as drug treatment) was calculated by summing up all normalized CPM values of associated PRSE by equation V.

$$\text{Normalized PRSE intensity}_{j,\,treated} = \text{sum}(\text{End CPM}_{j,\,k,\,treated}'') \qquad \text{(V)}$$

To calculate the change of normalized PRSE intensity of one gene upon drug treatment, we used equation VI.

$$\text{Change in normalized PRSE intensity}_{j,\,treated} = (\text{Normalized PRSE intensity}_{j,\,treated}) \,/\, (\text{Normalized PRSE intensity}_{j,\,untreated}) \qquad \text{(VI)}$$

To quantify whether such change was significant or not, we assessed the technical noise of this process (from 3'-end-seq library construction, sequencing to computation) via calculating the change in normalized PRSE intensity of one gene between two replicates without drug treatment. In particular, we replaced all "treated" terms mentioned above with the corresponding term from another "untreated" replicate, resulting in "change in normalized PRSE intensity$_{j,\ untreated}$". As expected, the changes in normalized PRSE intensity between two drug-free replicates from all genes followed a normal distribution centered around zero (**Figure 3e**, "0 min").

For convenience, we referred to the term— "change in normalized PRSE intensity" defined here— still simply as PRSE intensity in this paper. We compiled a comprehensive list of PRSE intensity in each gene for all drug-treated samples compared with the 0 min samples (**Supplementary Table 8**).

RNA-seq coverage normalization to show genome-wide gene expression polarity

To quantify gene expression polarity at genome scale from RNA-seq data, we adopted a computational process to normalize RNA-seq coverage across all genes similar to previously described[77]. RNA-seq coverage per nucleotide was first calculated by bedtools in a strand-specific manner (see "NGS data processing" subsection in **Methods**). Then, according to annotation (NC_000913.3), 5% length from 3' of noncoding genes was trimmed in this analysis to eliminate intrinsic transcription termination (in principle on the last nucleotide of the noncoding genes), which introduced noise to the coverage analysis; And all CDSs were kept for protein-coding genes,

as intrinsic transcription termination occurred outside CDSs. Then, the length of each gene was rescaled to 0 to 1 and 100 equally spaced points were generated along transcription direction. RNA-seq coverage on each of these points between 0 to 1 was computed via linear interpolation based on read coverages of the two nearest nucleotides. New coverage data was averaged across all gene and finally normalized by dividing the maximum value of these 100 points (**Figure 5a**, **5b**).

PRSE profile rescaling in a gene-wise manner

To visualize PRSEs of each gene before and after drug treatment in an unbiased manner (**Figure 5c-5f**), we adopted a computational approach to rescale the PRSE profile for each gene across different conditions. For each gene, the PRSE profile was defined as the vector of the CPM values of the 3' end at each nucleotide along this gene. As mentioned above (see "RNA-seq coverage normalization to show genome-wide gene expression polarity" subsection in **Methods**), for noncoding genes, nucleotides from the last 5% length proximal to their 3' ends were trimmed. Here for each gene, we focused on two PRSE profiles, one at 0 min and another at 60 min of drug treatment. For each gene, we first processed its PRSE profile at 60 min by dividing gene expression change between these two conditions ($TPM_{60\ min}$ /$TPM_{0\ min}$ in RNA-seq data); the corresponding PRSE profile at 0 min was kept constant. Therefore, we removed the undesired impact of gene expression change on PRSE profile. Next, for each gene, its nucleotide sequence was equally divided into 50 segments along the transcription direction; Within each segment, the processed CPM values of all nucleotides belonging to this segment was summed. Thus, we converted the original PRSE profiles of different genes with different length to new profiles with uniformly 50 elements. Finally, for each gene, the processed PRSE profiles of the two samples (e.g., 0 min and

60 min) were rescaled to [0, 1] by dividing the maximum value among all 100 values. The rescaled PRSE profiles were used in visualization (**Figure 5c-5f**).

Analysis of PSRE intensity flanking mutation sites

Here, we assumed that gentamicin-induced mutations were positionally enriched on PRSE-prone regions of a coding gene. On the other hand, spontaneous mutation sites were irrelevant to PRSE intensity. To test this hypothesis, we first excluded the mutation events corresponding to mobile elements from this analysis, as these mutation are inherently mobile and their origins are hard to track. Next, we focused on mutations that occurs uniquely within coding regions, where PRSEs are relevant. This results in 29 (out of 35) gentamicin-induced mutations that are within 21 genes, and 8 (out of 24) spontaneous mutations that locate in 8 genes. All relevant nucleotides on the chromosome of deletion or insertion or BPS positions are defined as mutation sites. We then assessed the PRSE intensity flanking each mutation site, via two different computational strategies.

First, we calculated normalized PRSE intensity in the CDS region of genes harboring the corresponding mutations. To this end, we summed up the intensity of PRSEs in relevant genes and normalized this value by the length of CDS (equation VII). Therefore, this metric reflects the averaged PRSE signal per nucleotide in the CDSs of genes where the mutations occur. Equation VII is used to generate **Figure 4f** (60 minutes after gentamicin treatment) and Supplementary **Figure 13** (all time points).

Normalized PRSE intensity (gene-level) = ∑(End CPM of PRSEs)/gene length (VII)

As the CDS sizes vary across genes, we are also interested in exploring whether some local PRSEs contribute more to the induced mutagenesis. To this end, we defined a window flanking the mutations with a fixed size, and quantified whether PRSE signals in this window substantially exceed the signals across the CDS of the corresponding gene (**Supplementary Figure 14a**). Equation VIII is adopted to derive the local PRSE intensity flanking the mutation site.

Normalized PRSE intensity (site-level) = (∑(End CPM in window)/window length)/(∑(End CPM in this coding locus)/CDS length) (VIII)

Since we introduced a window flanking the mutation site (see equation VIII) in order to calculate the local PRSE intensity flanking the mutation site, we also investigated whether the length of this window leads to any bias in this analysis. Three different window length settings are tested: 25 nt, 51 nt and 101 nt (**Supplementary Figure 14b**). The results suggest that the correlation between gentamicin-triggered mutations and local PRSEs depends on the specific window length. Particularly, in all cases, local PRSE signals flanking gentamicin-triggered mutations are stronger or at least comparable to those flanking spontaneous mutations. The strong correlation between gentamicin-triggered mutations and heighted local PRSE signals is more profound when the window length is smaller than 101 nt, indicating that a local effect exists that flanking PRSEs contribute to induced mutagenesis (**Supplementary Figure 14b**). However, we also note that such local effects only apply to a few mutations (n = 6), indicating that both proximal (**Supplementary**

Figure 14b) and more distant PRSEs (**Figure 4f, Supplementary Figure 13**) contribute to induced mutagenesis. The underlying mechanisms remain to be elucidated.

RNA structure and sequence analysis

For RNA secondary structure analysis, RNA sequence of 50 nt upstream the location of each predominant PRSE was extracted from *E. coli* genome NC000913.3 and subjected to RNAfold command line tool[78] (2.4.18) with parameters '--noPS --noconv -C' to predict minimal free energy (MFE) of RNA folding. For RNA sequence analysis, a home-made python script was adopted to calculate and plot the motif logo of upstream 10 nt sequences of the predominant PRSEs. Here we defined the nucleotide positions of predominant PRSEs or intrinsic termination sites as +1 (**Figure 5h-j**).

Data and software availability

The raw data of 3'-end-seq was deposited to GEO (GSE234254, currently kept private with a token for the access of reviewers: ingrkmuixhwntsd). The raw data of survived isolate genome re-sequencing was deposited to SRA (PRJNA982572). Other materials that support the findings of this study are available upon reasonable request.

Acknowledgements

We thank Keyong Sun for providing protocol of genome re-sequencing. We thank Chengxia Zheng and Weifeng Zhang for their technical suggestion on hybridization assay of R-loop and

PFGE. JL was supported by the Tsinghua-Peking Center for Life Sciences. TW was supported by the National Natural Science Foundation of China (32100071), and the ShanghaiTech Startup program.

Author contributions

TW conceived and designed the project with the critical input from YZ and RC. YZ performed genetics, biochemistry, cell sorting and genome re-sequencing experiments facilitated by TW and ZX. RC established 3'-end sequencing method, profiled transcription dynamics with the help of TW, YH and PS. RC and TW performed computational analysis of the 3'-end-seq and genome re-sequencing data. YZ and TW analyzed data from other experiments. TW, YZ and RC wrote and revised the manuscript. JL provided suggestions in manuscript revision. TW and JL supervised and funded the project.

Competing interests

The authors declare no competing interests.

Figures and Captions

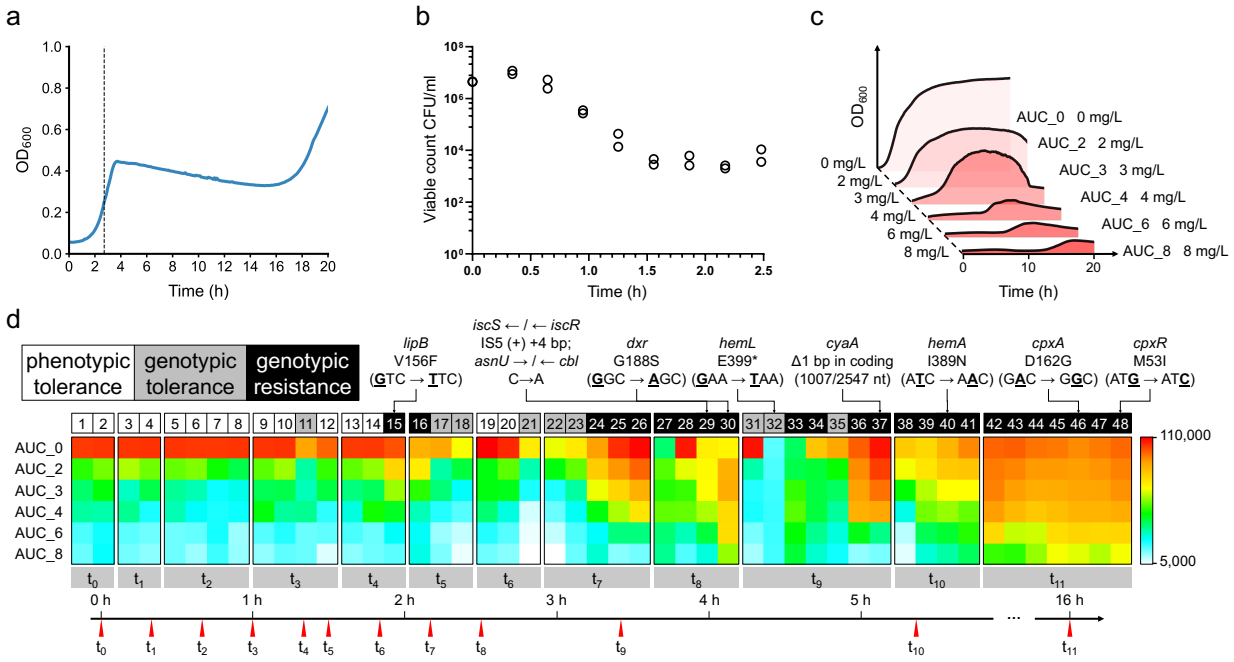

Figure 1 Survival modes switched rapidly from phenotypic tolerance to genetic resistance under gentamicin treatment. **(a)** Growth curve measured by OD_{600} of *E. coli* treated with 6 mg/L gentamicin. The dash line indicates drug treatment. **(b)** Lethality of gentamicin quantified by time-kill curve of *E. coli*. **(c)** A schematic of the drug susceptibility assay. Isolates were cultured in medium containing gentamicin of different concentrations. For each concentration, AUC of growth curve was quantified and was indexed as "AUC_x" (x = 0, 2, 3, 4, 6 and 8, corresponding to gentamicin concentration in mg/L). **(d)** Drug susceptibility of all isolates. Heatmaps show AUCs (drug susceptibility assay encoded by color bar on the right, OD_{600} × second) of 48 isolates recovered during gentamicin treatment (t_0 ~ t_{11}). The timings of sampling are labeled in the time track below. Isolates are manually categorized into phenotypic tolerance (WT), genotypic tolerance (prolonged lag in the absence of gentamicin), and genotypic resistance (larger AUC under gentamicin) (see **Methods**); These categories are highlighted by three colors (white, grey

and black) above heatmaps. Mutations identified by resequencing from eight selected isolates are listed above.

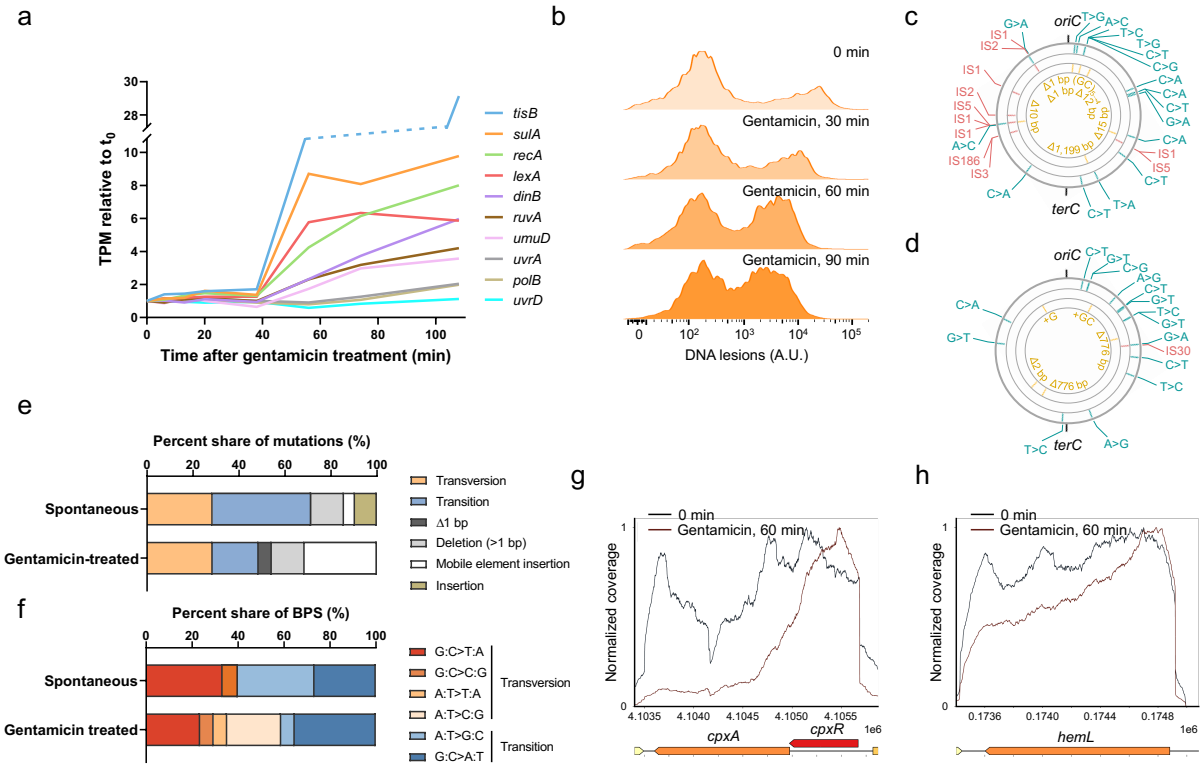

Figure 2 Genomic instability and induced mutagenesis were triggered by gentamicin. **(a)** SOS responses were activated during gentamicin treatment. Shown are the fold changes of transcripts per million (TPM) of representative genes in SOS regulon measured by RNA-seq. **(b)** Gentamicin induced DNA damage. DNA damage levels at 0 min, 30 min, 60 min and 90 min post gentamicin addition measured by TUNEL assay and flow cytometry. Positive cell ratio: 0 min, 31.3%; 30 min, 36.6%; 60 min, 48.2%; 90 min, 50.9%. **(c)** Mutations emerged after gentamicin treatment and **(d)** spontaneous mutations. Their genomic positions were indicated; The genomic positions of *oriC* (3,925,744 – 3,925,975) and *terC* (1,609,157 – 1,609,179) were labeled for reference. **(e)** Distinct mutation spectrums between spontaneous mutations (**Methods**) and isolates survived in gentamicin treatment for three hours or longer (**Methods**). Shown are proportions of mutations belonging to different categories. Shown in **(f)** are zoom in of BPSs in **(e)**. Examples from **(g)** *cpxRA* and **(h)** *hemL* operon show gene expression polarity towards 5' end of coding sequences

(CDS) triggered by gentamicin. Read coverages measured by RNA-seq at 0 min (black) and 60 min (red) drug treatment are presented.

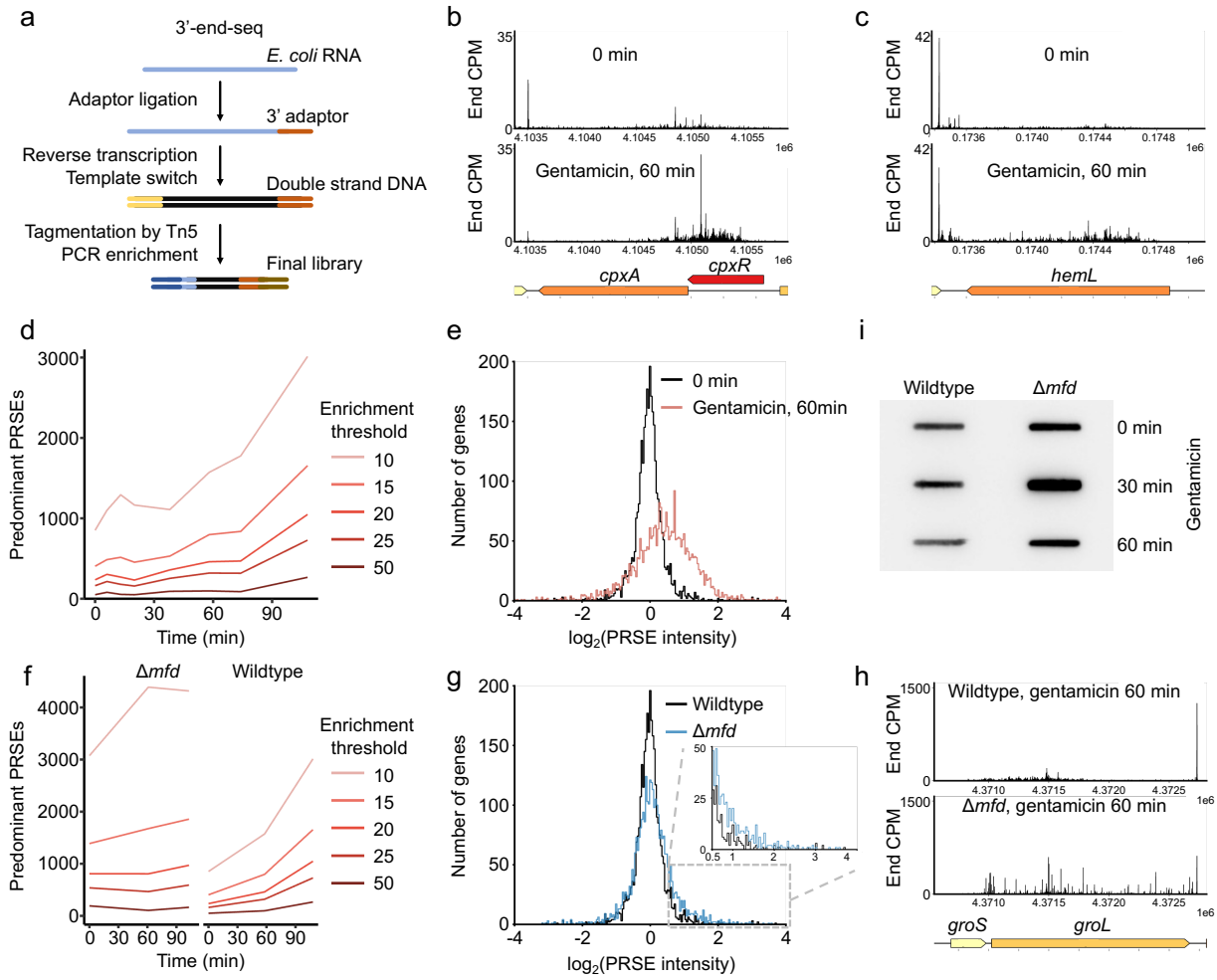

Figure 3 Gentamicin induced genome-wide PRSEs. **(a)** Schematics of 3'-end-seq workflows. **(b)** and **(c)** Gentamicin induced PRSEs across **(b)** *cpxRA* and **(c)** *hemL* operon. Profiles of 3'-end-seq show PRSEs in untreated (upper) and gentamicin-treated (lower) samples; Count per million (CPM, **Methods**) for 3' ends at each nucleotide on the strand of the gene transcription direction is plotted; Arrows below represent corresponding genes. **(d)** Predominant PRSEs increased during gentamicin treatment. The dynamics of predominant PRSEs under five thresholding criteria (**Methods**) are shown. **(e)** PRSE intensity increased during gentamicin treatment. The distribution of PRSE intensities (**Methods**) from 3,126 protein-coding genes are shown as histogram for comparison between 0 min and 60 min of gentamicin treatment ($P = 2.7 \times 10^{-159}$, one-sided Mann–

Whitney U (MWU) test). **(f)** Predominant PRSEs increased in Δ*mfd* strain. The dynamics of predominant PRSEs during drug treatment from Δ*mfd* and wildtype (the same as **(d)**) strains are shown. **(g)** PRSE intensity increased in Δ*mfd* strain without drug treatment. The distribution of PRSE intensities (**Methods**) from 3,126 protein-coding genes are shown as histogram to compare wildtype and Δ*mfd* strain at 0 min ($P = 3.6 \times 10^{-13}$, two-sided MWU test); Zoom in on the right tails of these two distributions are also presented to highlight the PRSE intensity increase in Δ*mfd* strain. **(h)** Knockout of *mfd* (lower) triggered stronger PRSEs than wildtype (upper) in specific loci under drug treatment. Profiles of 3'-end-seq show PRSEs across *groSL* operon after 60 min drug treatment, the settings are the same as **(b)** and **(c)**. **(i)** Knockout of *mfd* induced stronger R-loop formation than wildtype under gentamicin treatment. Shown are the gel images of R-loop blotting assay (**Methods**).

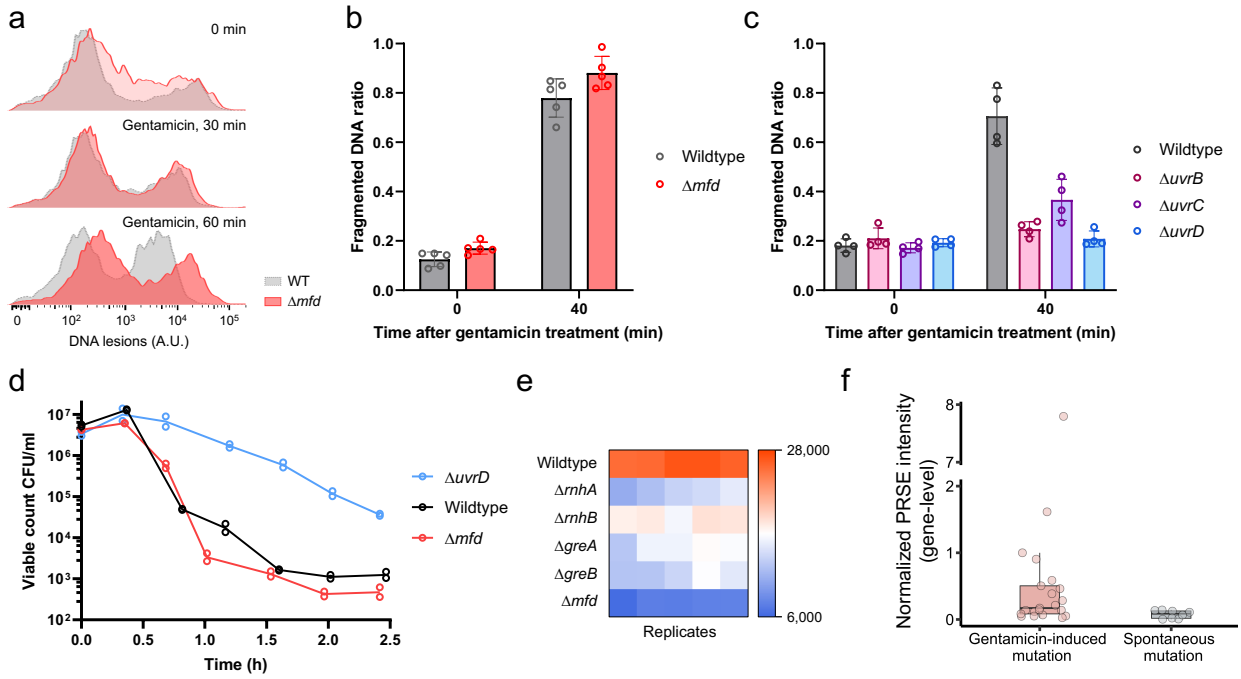

Figure 4 PRSEs are responsible for DNA damage and induced mutagenesis. **(a)** Δ*mfd* strain shows exacerbated DNA damage before and under gentamicin treatment. DNA damage levels of wildtype and Δ*mfd* strains at 0 min, 30 min and 60 min post gentamicin addition are measured by TUNEL assay. The FACS profiles of Δ*mfd* (red) are overlaid with that of wildtype (grey). **(b)** PFGE analysis (**Methods**) reveals more damaged genome in Δ*mfd* strain compared to wildtype upon gentamicin treatment. **(c)** Knockout of genes encoding RNAP pro-backtracking factors alleviate DNA damage under gentamicin treatment, characterized by PFGE assay. **(d)** The gentamicin lethality of transcription elongation factor gene knockout strains is consistent with their DNA integrity. Shown are two biological replicates of killing assay. **(e)** Knocking out genes encoding PRSE rescue factors leads to enhanced gentamicin susceptibility (**Methods**, AUC of growth curves of drug susceptibility assay, OD_{600} × second). **(f)** Genes carrying gentamicin-induced mutations are associated with higher intensity of PRSE signals, compared with genes harboring spontaneous mutations. The distributions of normalized PRSE intensity for these two groups of genes that carry

gentamicin-induced or spontaneous mutations (n = 21 and 8, respectively; **Methods**) after 60 min gentamicin treatment are shown as boxplot with scatters.

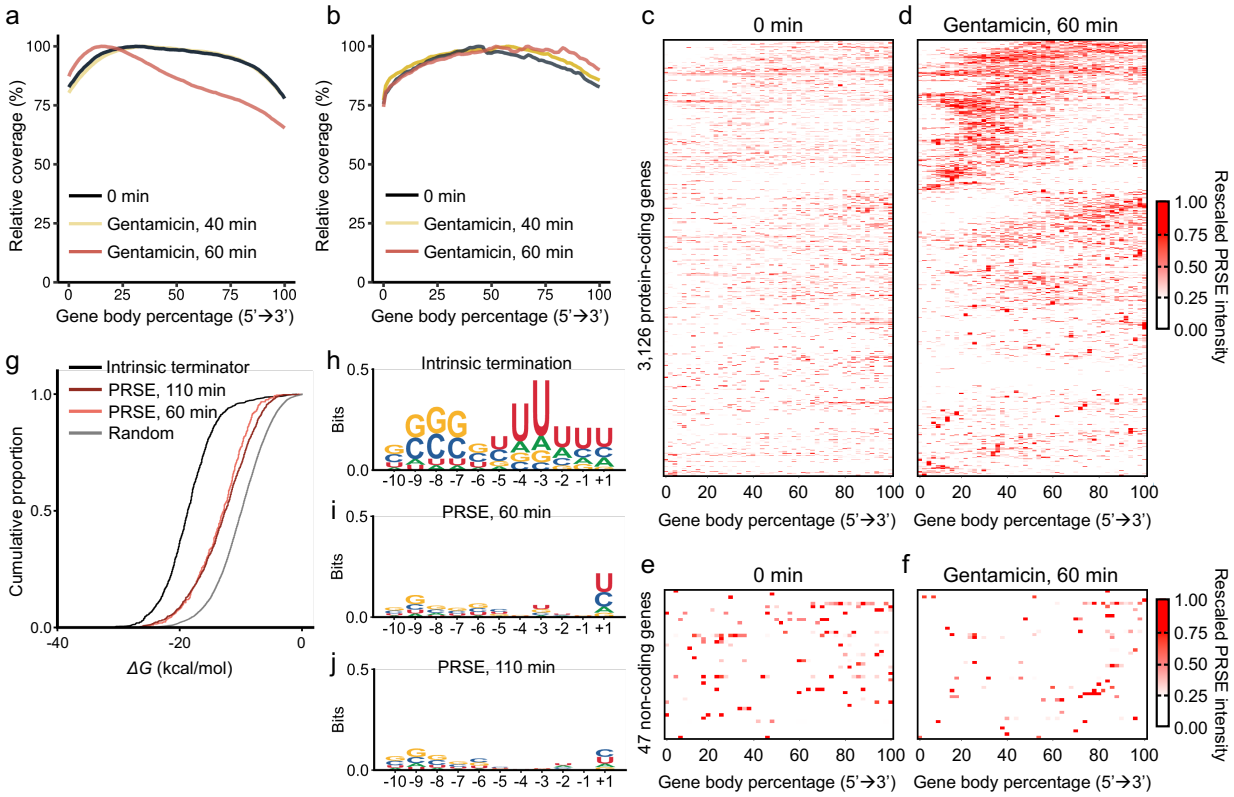

Figure 5 Genome-wide PRSEs are caused by the disruption of TTC and the derived structured nascent RNA. Genome-wide gene expression polarity towards 5' ends uniquely occurs in **(a)** 3,126 protein-coding genes, but not in **(b)** 47 noncoding genes. Read coverages measured by RNA-seq at 0 min (black), 40 min (yellow) and 60 min (red) drug treatment are presented. **(c)** - **(f)** Genome-wide PRSEs uniquely occur in protein-coding genes, but not in noncoding genes. Shown are rescaled PRSE intensities (**Methods**) in protein-coding genes at **(c)** 0 min or **(d)** 60 min; as well as in noncoding genes after **(e)** 0 min or **(f)** 60 min of gentamicin treatment. Each row represents one gene; Each gene is equally divided into 50 sections to visualize averaged PRSE intensity in each section; Rescaled PRSE intensities are encoded by color bar on the right. **(g)** Predominant PRSEs occur when RNAP produces structured nascent RNA that are originally disrupted by the coupled ribosome. The cumulative curve of MFEs from random 50mers on *E. coli* genome (n = 10,000) is shown as negative control; MFEs of 1,330 intrinsic terminators (50 nt upstream,

enrichment cutoff = 20; **Methods**) are shown as positive control; Also shown are MFEs for predominant-PRSE-associated nascent RNAs (the same cutoff as intrinsic terminators) at 60 min (n = 460; $P = 4.42 \times 10^{-84}$ vs. negative control; $P = 2.33 \times 10^{-15}$ vs. positive control) and 110 min (n = 1048; $P = 1.41 \times 10^{-105}$ vs. negative control; $P = 2.78 \times 10^{-15}$ vs. positive control) of drug treatment. Two-sided Kolmogorov-Smirnov test was used to compare MFEs from different groups. **(h) - (j)** PRSEs emerged at loci with poor intrinsic termination signal. Motif analysis of nascent RNA associated with the predominant PRSEs in **(g)**. Shown are **(h)** intrinsic terminators, **(i)** PRSEs in 60 min and **(j)** 110 min of drug treatment.

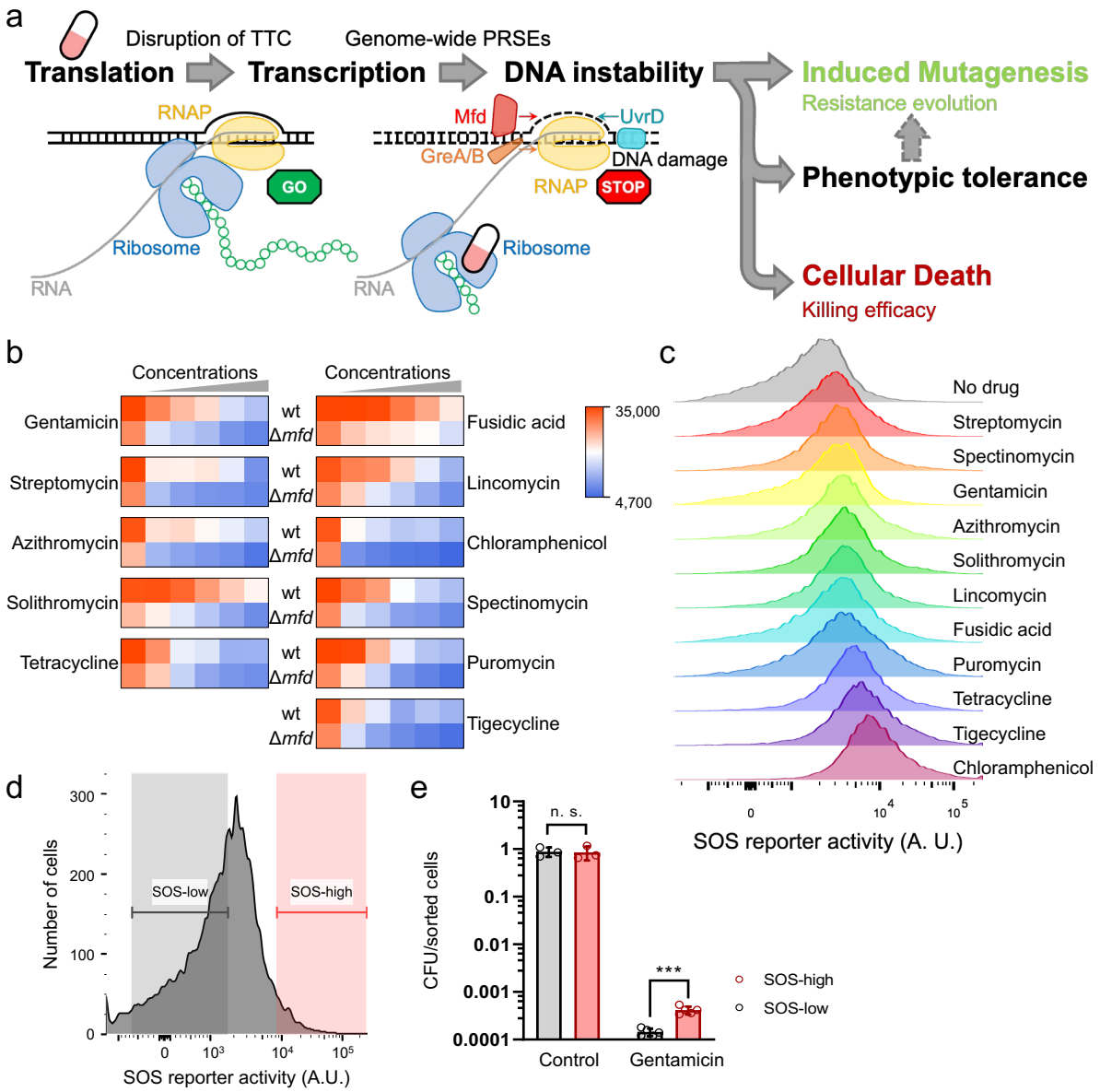

Figure 6 The reverse-central-dogma pathway is universal to the efficacy of ribosome antibiotics. **(a)** Schematics of the reverse-central-dogma pathway uncovered here. **(b)** The pathway pervasively contributes to bacterial fitness upon ribosome antibiotics treatment. Shown is the susceptibility assay (**Methods**, AUC of growth curves, OD_{600} × second) of either wildtype or Δ*mfd* strain to a panel of ribosome antibiotics. **(c)** Ribosome antibiotics universally trigger SOS responses, measured by flow cytometry analysis of the SOS reporter strain after treatment by

ribosome antibiotics (**Methods**). (**d-e**) Hyperactivation of SOS responses at the single cell level enhances the phenotypic survival of bacteria upon gentamicin treatment. **(d)** Schematics of FACS to sort either SOS-high or SOS-low subpopulation. **(e)** The survival rates of sorted subpopulations are shown (P = 0.00008, two-tailed t test).